We are IntechOpen, the world's leading publisher of Open Access books Built by scientists, for scientists

6,900
Open access books available

186,000
International authors and editors

200M
Downloads

Our authors are among the

154
Countries delivered to

TOP 1%
most cited scientists

12.2%
Contributors from top 500 universities

WEB OF SCIENCE™

Selection of our books indexed in the Book Citation Index in Web of Science™ Core Collection (BKCI)

Interested in publishing with us?
Contact book.department@intechopen.com

Numbers displayed above are based on latest data collected.
For more information visit www.intechopen.com

3

Tapping Mode AFM Imaging for Functionalized Surfaces

Nadine Mourougou-Candoni
CNRS, Aix-Marseille University, CINaM
France

1. Introduction

The tapping mode in Atomic Force Microscopy (AFM) is a key advance in AFM technology for functionalized surface imaging. In fact, the basic technique of AFM, which is contact AFM, is not well adapted to examine such surfaces due to problems of friction and adhesion. Therefore, the tapping mode of operation was developed to overcome drawbacks of contact mode (Binnig et al, 1986). This mode uses oscillation of the cantilever tip at or near its natural resonant frequency while allowing the cantilever tip to impact the target sample for a minimal amount of time. This intermittent contact lessens the damage done to the soft surface and to the tip, compared to the amount done in contact. Thus, the tapping mode is the method of choice for imaging functionalized surfaces. A functionalized surface is a solid surface where molecules have been adsorbed leading to various patterns, from isolated molecules dispersed on the surface to homogeneous films. The patterns provide ideal platforms for the immobilization or recognition and specific interaction of biomolecules. In the preparation of functionalized surfaces, the first process consists in understanding the mechanism of adsorption. The aim is to yield good orientation and stability of the immobilized molecules, thus leading to high-functionality of the surface for applications, such as biosensors.

The purpose of this chapter is to highlight potentialities of AFM in the tapping mode, for imaging functionalized surfaces in air. Therefore, we explore quantitative and qualitative information given by AFM during processes of functionalization of substrates by molecules. For the substrate, the surface must be as flat as possible in order to reach high resolution imaging. Indeed, a molecule of a diameter of a few nm placed on a surface of a roughness of a few nm would not be visible in an AFM height image as it would be "hidden" by the surface topography. Thus, we focus on mica which presents a surface with atomically flat terraces. Concerning molecules, they range from more or less modified alkane chains to derivatives of DNA. Hence, we study the immobilization of single molecules and the formation of self-assembled monolayers (SAMs) and polymerized films. In the resulting pattern, molecules either adsorb by physical binding, e.g. via counter ions or hydrophobic interaction, or form covalent bonds on the surface.

We start with a brief description of the topographical mode of tapping AFM. Then, various illustrations of surface functionalization are investigated by AFM imaging. In the last part, we present improvements on conventional AFM in tapping mode.

2. Topographical imaging with AFM taping mode

2.1 Principle of AFM in tapping mode

In tapping mode, the AFM scans the sample surface with a very tiny and sharp tip mounted at the end of a flexible cantilever. The tip is oscillated and moved towards the sample (Binnig et al., 1986). Only intermittently touching or "tapping" occurs on the sample. Hence the dragging forces during scanning are greatly reduced (Tamayo & Garcia, 1996). Moreover, during oscillation, the tip goes through both the attractive and the repulsive regions of the tip–sample force field. In case of functionalized surfaces, AFM parameters are selected to minimize modification of the surface caused by moving or removing molecules which are loosely bound to the surface and easily damageable.

The cantilever is mounted to a piezoelectric actuator (figure 1). A position sensitive photo detector receives a laser beam reflected off the end-point of the beam to provide cantilever deflection feedback. During the scan of the tip over the sample surface with feedback mechanisms, PZT scanners enable to maintain the tip at a constant force or a constant height. The operation mode called constant force is the most common in tapping AFM. Thus, the tip is moved up and down with the contour of the surface and the laser beam deflected from the cantilever provides measurements of the difference in light intensities between the upper and lower photo detectors.

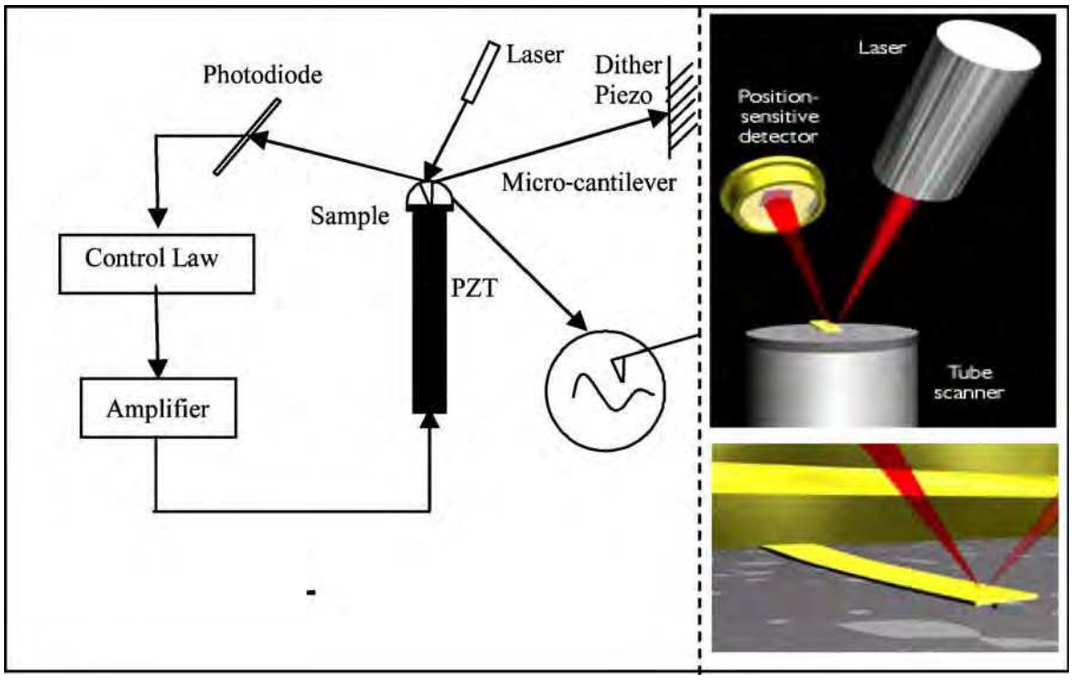

Fig. 1. Schematic of basic AFM operation (left), real micro-cantilever and components (right) (Jalili & Laxminarayana, 2004).

The PZT actuator applies a force on the cantilever base and makes the cantilever tip vibrate. The frequency of oscillation is fixed near the resonance of the tip and the oscillation amplitude is monitored. Starting from free oscillation amplitude, the sample is approached to the tip until its amplitude is reduced to the set point value, which is selected to reduce

damage to the sample. When the tip-sample gap is in the nanometer range, the oscillation amplitude is damped by tip-sample repulsive interactions that occur each cycle, due to energy loss (figure 2). Then the oscillation amplitude is kept at the set point by adjusting the vertical (z-axis) position of the tip with a piezoelectric drive. Therefore, the vertical motion is controlled by the feedback mechanism, which allows the adjustment of the signal to keep the amplitude constant. The variations of the z-position of the tip during scanning are plotted as a function of the xy position of the tip to create the height image, in which gray or color contrast is used to show the z-variations. Thus, the reduction of the oscillation amplitude due to interactions with molecules of the surface is generally used to identify and measure surface topographic features.

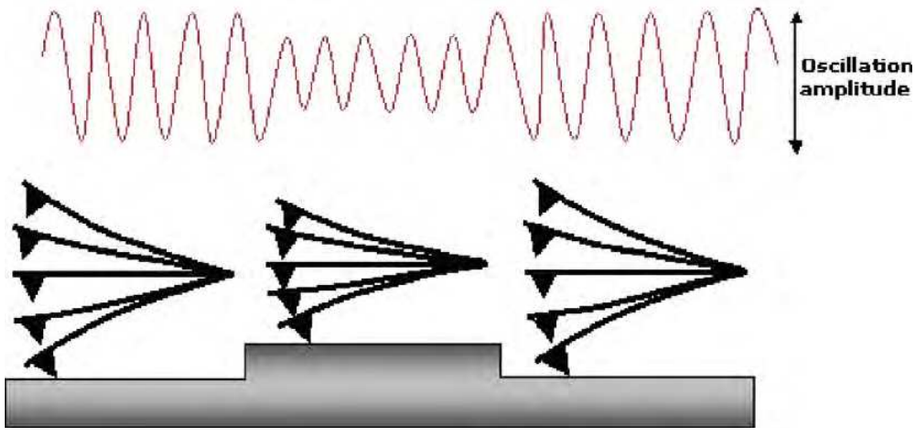

Fig. 2. Schematic representation of an AFM tips operating in the tapping mode (Alessandrini & Facci, 2005).

2.2 Parameters influencing topographic imaging

In topographic imaging, the lateral resolution is given by the radius of curvature of the tip. However, using commercial cantilevers with a 10 to 50 nm radius of curvature for the tip, surprisingly permits to acquire (sub)-nanometer resolution on reconstituted surface. In fact, the resolution is higher than that expected on the basis of radius of curvature, due to the presence of nano-scale asperities extending irregularly from the tip. In this case, the asperities may play the role of the true imaging tip (Müller et al., 1999). Moreover the shape of the tip also plays an important role in the resolution. A common source of artifacts appears when height variations are in the range of the tip's radius of curvature, i.e. 10 to 50 nm. Then, the sample interacts with the sides of the probe. The resulting image is a combination of the real sample topography and the tip geometry, hence broadening the surface features. Another common problem is the shadowing or multiplication of small structures produced by multiple probe effects. These are due to the presence of multiple asperities on the tip apex, which usually originate from contamination.

Another important parameter influencing image resolution is the type of sample. The sample preparation procedure must be chosen so as molecule-surface interaction is always stronger than tip-molecules interaction. In fact, the spatial resolution increases with hardness and flatness of the sample. This is due to long-range forces, which play a significant role. They involve a huge number of atoms contributing to the contrast formation

mechanism, even if true atomic resolution images have been obtained by the AFM on layered samples (Ohnesorge & Binnig, 1993). In the case of soft or damageable functionalized surfaces, the resolution crucially depends on the softness of the sample. Hence, cell membranes induce a resolution in the range of a few tens of nanometers. For isolated molecules like proteins, the resolution can be improved to few nanometers. Concerning the choice of the substrate, popular substrates are glass, silicon or mica. We have selected mica because it exhibits the smoothest surface. In addition, thanks to the crystallographic structure of mica, a clean and very flat surface can be easily obtained by peeling off the outer leaflet of the surface using a simple cellophane tape. The smoothness of mica subsists when we cover it with gold by evaporation.

3. Imaging isolated molecules

In the case of functionalization with single molecules, we have been interested by oligonucleotides, i.e. pieces of single-stranded DNA. The functionalization of surface with these oligonucleotides is of great interest for the development of DNA chips, which are based on the capacity of oligonucleotides to recognize and to hybridize with their complementary strand. This method is widely used for the detection and characterization of genetic material for both clinical and environmental analysis. One critical aspect for the synthesis of such chips is the immobilization of oligonucleotides on the device surface. In fact, oligonucleotides must be available to hybridization without displaying rapid removal under hybridization or washing conditions.

3.1 Preparation of the substrate

Generally, the immobilization of oligonucleotides is achieved by covalent coupling with the surface. It requires activation with a cross-linking reagent and/or modification of the oligonucleotide with a reactive group. Several studies have been carried out on Si/SiO_2 surfaces (Chrisey et al., 1996; Cloarec et al., 1999), on gold surfaces (Herne & Tarlov, 1997; Steel et al., 1998; Kelley et al., 1998; Lisdat et al., 1999; Huang E. et.al, 2001) or on mica (Hansma et al., 1996; Shlyakhtenko et al., 1999). Among these substrates, we have chosen mica for its flatness and we have covered it with gold in order to adsorb thiol-functionalized oligonucleotides via gold-sulfur bond. In fact, this linkage allows configurational freedom for oligonucleotides to form a double helix with the complementary molecule. Therefore, mica is covered with gold by evaporation in an UHV chamber at a rate of 1-2 Å s^{-1} for a surface temperature of 460 °C, the film thickness being monitored by a quartz microbalance (Klein et al., 2000). In figure 3, AFM images of Au (111) surface shows atomically flat terraces of 500 nm (figure 3a) and presence of atomic steps (figure 3b). It must be pointed out that these terraces and steps correspond to the structure of mica.

3.2 Functionalization with isolated molecules

Previous works on the adsorption of thiolated oligonucleotides on gold substrates used surface chemical analysis techniques such as Surface Plasmon Resonance (SPR) (Herne & Tarlov, 1997), X-ray Photoelectron Spectroscopy (XPS) (Levicky et al., 1998), neutron reflectivity (Steel et al., 1998) or electrochemical quantitation (Peterlinz et al., 1997). However these techniques give only the average structure of the oligonucleotide. The

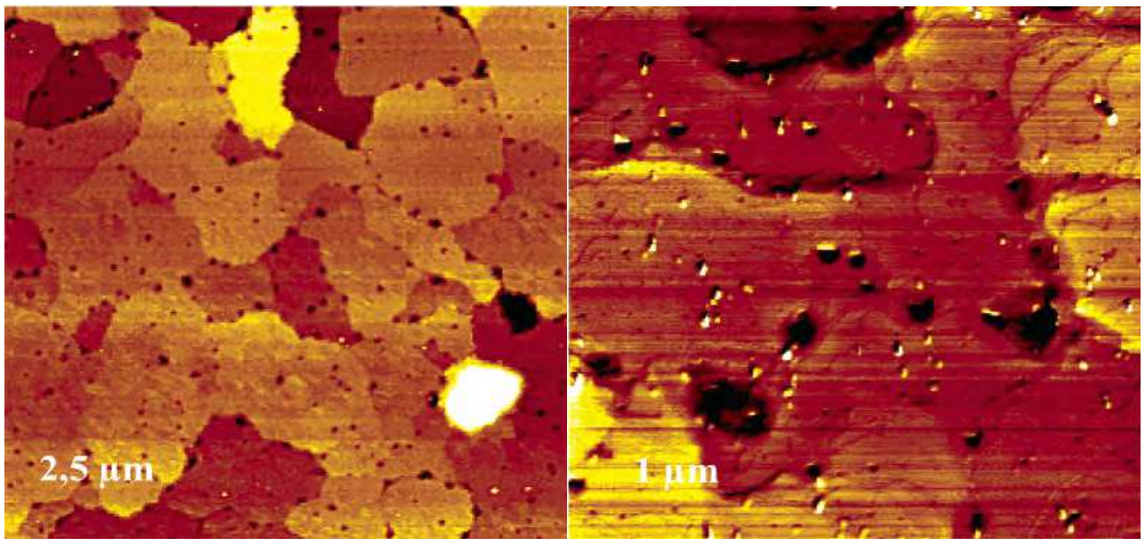

(a) (b)

Fig. 3. AFM images of an Au(111) surface obtained by electron evaporation of gold on mica sheets in a UHV chamber at an evaporation rate of of 1-2 Å s^{-1} for a substrate temperature of 460 °C: 3a) Atomically flat terraces of 500 nm are observed with a size of scanning of 2.5 µm × 2.5 µm; 3b) Atomic steps are distinguished with a size of scanning of 1 µm × 1 µm,.

advantage of AFM imaging in the tapping mode is achieving a direct visualization of surfaces to study the adsorption process without modifying the surface. Therefore, we have performed AFM experiments in an ambient atmosphere, typically 20-25 °C and 30-35 % humidity, using the tapping mode of AFM at a scan frequency of 1-2 Hz. Surface topography has been obtained with uncoated silicon cantilever tips of ~ 15 nm apex diameters. Then our AFM images have been processed with flatten and contrast enhancement processing from Nanoscope III software. Figure 4a shows a 1 µm wide AFM image of a surface exposed for a few seconds to oligonucleotides by immersing in a solution at a concentration of 5 nM in KH_2PO_4 (1 M). This surface exhibits particulates with a height of ~1 nm and a diameter of 15 nm.

How do we attribute these particulates to oligonucleotides? On one hand, oligonucleotides of 25 bases adsorbed on the gold surface through the thiol group and stretched to full length are higher than 16 nm according to SPR measurements (Herne & Tarlov, 1997). On the other hand, if the same oligonucleotide displays segments that are isotopically distributed in space, these authors estimated that the component of the radius of gyration along the direction perpendicular to the surface is on the order of $R_{gz} \approx 1.1 \pm 0.1$ nm (Steel et al., 1998). Thus, it appears that particulates observed by AFM (figure 4a) are oligonucleotides which are curled up in a ball. This globulate conformation of 25-bases oligonucleotides was also described by other authors with AFM (Hansma et al., 1996).

After a longer time of deposition, the surface becomes more covered in particulates, i.e. in oligonucleotides; nevertheless oligonucleotides are still well-distinguishable (figure 4b). In figure 4b, adsorption is inhomogeneous since the molecules are arranged like filaments which seem to follow lines displayed by the surface. Sometimes these lines reproduce the

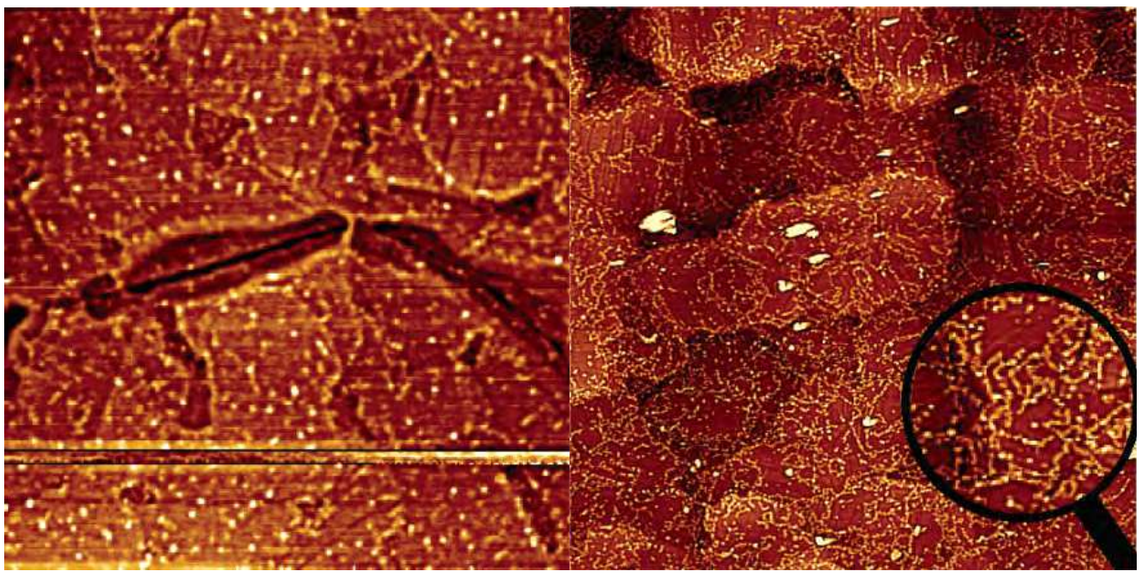

(a) (b)

Fig. 4. AFM images of surfaces exposed to oligonucleotides (5 nM) in a solution of KH2PO4 (1 M): 4a) for a few seconds: the surface exhibits particulates with a height of ~1 nm and a diameter of 15 nm. The size of scanning is 1 μm × 1 μm. 4b) for 10 min: the particulates form a filamentous arrangement following the symmetry of the Au(111) surface (zoom inset). The size of scanning is 2 μm × 2 μm.

symmetry of the Au(111) surface (see the magnified area). Thus, molecules seem to adsorb preferentially at the structure of the surface due to the presence of steps and/or in reconstruction areas. We must emphasize that molecules adsorbed on these lines seem to be connected together because they are close-packed and the lateral resolution of the AFM is limited.

3.3 Physisorption or chemisorption

During contact between the surface and oligonucleotide, molecules are either chemisorbed, i.e. specifically adsorbed via gold-sulfur linkage, or physisorbed, i.e. non-specifically adsorbed via nitrogen interactions of nucleotide side chains. We have studied non-specific adsorption with non-thiolated oligonucleotides. According to Auger Electron Spectroscopy (AES), non-thiolated oligonucleotides are detected whereas AFM images do not display bumps. Thus, bumps observed with thiolated oligonucleotides are due to the linkage through thiol and non-specifically adsorbed molecules are not visible with AFM. This is probably due to the diffusion of non-attached molecules on the surface, which is more rapid than the scanning speed of AFM (Mourougou-Candoni et al., 2003).

How do oligonucleotides adsorb on the surface? As molecules do not have enough time to react with the surface, they are essentially physisorbed, and they reach their equilibrium density in a few seconds. After the surface is removed from the solution, these molecules diffuse and react with the surface becoming chemisorbed. According to our images, this chemisorption is promoted by steps or/and reconstructions of the surface.

3.4 Kinetic of adsorption

The acquisition of AFM images with time of deposition shows clearly that adsorption proceeds in two steps (Mourougou-Candoni et al., 2003):

- In the first step, molecules adsorb instantaneously with a density of 10^{11} molecules cm^{-2} that we are able to count on AFM images (figure 4a). This density cannot be explained by diffusion of oligonucleotides during immersion in solution because their coefficient of diffusion of (6-7) $\times 10^{-7} cm^2\ s^{-1}$ (Tinland et al., 1997) is too low. In fact, we explain it by molecules reaching the surface during dipping.
- In the second step, the adsorption increases slowly with a rate of 10^8 molecules $cm^{-2}\ s^{-1}$ due to diffusion. This rate reflects the chemisorption of oligonucleotides. The kinetic factor of $4\times10^{-4}\ s^{-1}$ is consistent with the measures for chemisorption of alkanethiol on a gold surface (Lavrich et al., 1998). Considering that this factor is around $(10^{13}\text{-}10^{14}) \times e^{-E/RT}\ s^{-1}$, we obtain an activation energy, E, around 100 kJ mol^{-1}. This is in the range of the activation energy of surface molecule dissociation. Thus, it corresponds to the reaction activation energy of the thiol group with gold. In addition, the reaction rate can depend on the structure of the surface as displayed by AFM images (figure 4b).

In this two-step mechanism, the density of chemisorbed molecules is proportional to the equilibrium density of physisorbed molecules. Therefore, during incubation in water at ambient temperature, physisorption being limited by electrostatic repulsion between neighboring oligonucleotides due to negative charges of their phosphated backbone, it induces a low chemisorption. Moreover, this chemisorption must be increased by promoting physisorption. Indeed, electrostatic are minimized in our solutions with phosphate KH_2PO_4 (1M) due to high ionic force, which permits to screen oligonucleotides charges. However, we have observed that chemisorption also increases in water at high temperature (60 °C). Thus the electrostatic repulsion described as a limiting factor (Steel et al., 1998) is not sufficient here. In fact, the activation energy that we have calculated gives a kinetic factor for specific reaction 100-fold higher at 60 °C than at room temperature.

Furthermore, the densities of molecules evaluated in these images are drastically different from the values obtained by Huang et al. (Huang E. et al., 2001). With a gold surface similar to ours and with same concentrations, they estimated from their AFM images a density in the 10^9 molecules cm^{-2} range. In fact, they consider some large lumps appearing with a diameter of 26-40 nm as oligonucleotide molecules, which we would attribute to impurities as those visible in figures 4 (or packs of oligonucleotides). However, their AFM images display small features they do not take into account and that we assign to oligonucleotides.

In conclusion, we show that AFM permits to study the adsorption process of isolated molecules such as oligonucleotides on a surface, here gold surface. Indeed AFM in tapping mode provides a direct visualization of oligonucleotide-coupled surfaces with a nanoscopic resolution. In addition AFM coupled with chemical analyses contribute to differentiation between physisorption and chemisorption. Thus, chemisorbed oligonucleotides appear as white bumps of 1 nm height that we can count on the gold surface. In addition, AFM exploration leads to determination of adsorption kinetics in a two-step mechanism. The first instantaneous adsorption concerns essentially molecules, which adsorb non-specifically during dipping of the substrate, reaching their equilibrium density. Then, their reaction

with surface is promoted by steps and/or reconstructions of the surface. The increase of density observed in the second step concerns molecules physisorbing from solution and reacting with the surface by diffusion. Finally, AFM allows us to show that this reaction depends on the structure of the surface and to evaluate a kinetic factor increasing with temperature.

4. Imaging self-assembled monolayers

Following the previous work on functionalization of surface with oligonucleotides, we have been interested by using them for hybridization with DNA strands. Therefore, oligonucleotides must be available to hybridization without displaying rapid removal under hybridization or washing conditions. It means that oligonucleotides must be chemically grafted on the surface. Indeed, thiol-metal bonds are on the order of 100 kJ mol^{-1}, making the bond stable in a wide variety of temperature, solvents, and potentials (Vos et al., 2003). Thus for further applications, we have passivated a surface functionalized with a high density of oligonucleotides, using SAMs.

4.1 What is called self-assembled monolayer?

Self-assembled monolayer, or SAM, provides one of the easiest ways to obtain ordered monolayers leading to the preparation of thermodynamically stable monolayers (Nuzzo & Allara, 1986; Ulman, 1991; Dubois & Nuzzo, 1992) as compared to Langmuir–Blodgett (Vos et al., 2003; Madou, 2002) and other techniques, where only physisorbed, thermally unstable mono/multilayer films are obtained. They consist of a monomolecular thick film of organic molecules, which presents a hydrophilic "head-group" and a hydrophobic "tail group". The formation of SAM starts by strong chemisorption of the hydrophilic "head-group", from either vapor or liquid phase (Schwartz, 2001), followed by a slow two-dimensional organization of hydrophobic "tail groups" (Wnek & Bowlin, 2004).

Areas of close-packed molecules nucleate and grow until the surface is covered with a single monolayer. In fact, the monolayer packs tightly due to Van der Waals interactions (Kaifer, 2001; Estroff et al., 2005). Several studies show that long-chain alkane thiols form more well-ordered defect-free monolayers (hydrophobicity increases with the length of alkanethiols) than short-chain alkanethiols, disulphides or sulphides. Aromatic (pi systems like benzene, naphthalene or diphenylene systems) or/and hydrogen-bonded molecules with multiple contacts, containing functional groups like thiols, amines, sulphides, selenides etc. provide improved stability (Bandyopadhyay et al., 1999; Venkataraman et al., 1999; Aslam et al., 2001).

4.2 Passivation with self assembled monolayer

One of the important advantages of SAM is that they can be prepared in the laboratory by simply dipping the desired substrate in the required millimolar solution for a specified time followed by thorough washing with the same solvent and drying, often using a jet of dry argon. In our work, we have investigated the influence of physico-chemical properties of molecules forming the SAM. Therefore, we have carried out passivation of oligonucleotides functionalized gold surface obtained above with SAM. An important property of molecules forming SAM is that they display a hydrophilic "head-group" and a hydrophobic "tail group", but also an "end group" at the end of the tail. This "end group" can be

hydrophobic or hydrophilic leading to what we call a "hydrophobic SAM" or a "hydrophilic SAM", respectively. Thus, we are interested by interactions between oligonucleotides and SAM according to properties of this "end group".

4.2.1 Passivation with hydrophobic SAM

One example of molecules which are known to form hydrophobic SAM on gold surface, are alkanethiols (containing ten methyl units), the "end group" being a CH_3. The monolayer formation proceeds in two steps: first physisorption and then diffusion and chemisorption, which lead to an ordered layer due to attractive intermolecular interaction. The balance sheet of these interactions induces a spontaneous and slightly exothermic (ΔE_{ads} 0.2eV) adsorption process of alkanethiols on a gold surface (Dubois & Nuzzo, 1992). We have observed that on surface functionalized with a high density of oligonucleotides (figure 5a), passivation leads to a homogeneous film of alkanethiols, compacting the oligonucleotides along lines (figure 5b). In figure 5b, the trend towards demixing is due to hydrophobic properties of alkanethiols, which push the oligonucleotides on the grain boundaries. Hence oligonucleotides are more or less upright on the surface with a height of several nm. However in this case, we note that passivation with a hydrophobic SAM renders the oligonucleotides not sufficiently available for hybridization, due to steric effects.

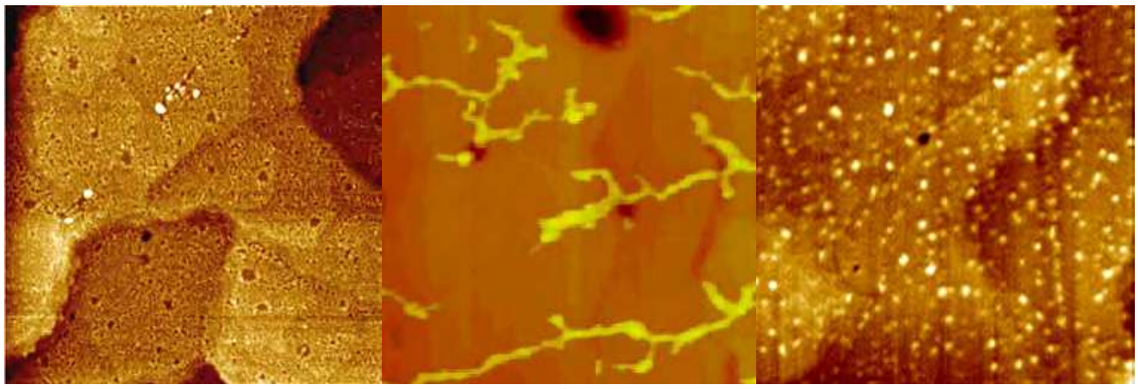

(a) (b) (c)

Fig. 5. Passivation of surface functionalized with oligonucleotides: 5a) AFM image of a surface functionalized with a high density of oligonucleotides: molecules cover the surface with holes of 1 nm depth. The size of scanning is 5 μm × 5 μm and z scale is 3 nm; 5b) AFM image of a surface after immersion in an aqueous solution of alkanethiol: oligonucleotides are grouped together and form compact lines of few nm height, surrounded by a homogeneous film of alkanethiols of 1 nm height. The size of scanning is 3 μm × 3 μm and z scale is 7 nm; 5c) AFM image of surface after immersion in an aqueous solution of mercaptohexanol: oligonucleotides show increased levels of desorption and the remaining molecules are dispersed on the surface. They appear as bumps of 1nm height, which are surrounded by a homogeneous film of mercaptohexanol. The size of scanning is 0.5 μm × 0.5 μm and z scale is 2 nm.

4.2.2 Passivation with hydrophilic SAM

The passivation with hydrophilic SAM has been carried out using mercaptohexanol, an alkylthiol chain containing six methyl units and an OH as "end group". We have observed

that this hydrophilic SAM desorbs almost all of the chemisorbed molecules (90%), substituting them by a molecular film (figure 5c). This result notably differs from the one obtained by other authors (Levicky et al., 1998), who measured 20 to 50% of desorption. They attribute these values solely to desorption of physisorbed oligonucleotides. In our case, the strong desorption is probably due to our gold surface with large terraces (figure 3a), where a highly ordered layer of mercaptohexanol can grow. In contrast, their surface of gold evaporated on glass at low temperature shows nanometric crystallites. Hence the organization of their layer of mercaptohexanol is not sufficient to compete with chemisorbed oligonucleotides. In conclusion the passivation with a hydrophilic molecule leads to a surface with only few oligonucleotides, which are well-isolated for further hybridization with a DNA stands.

4.3 Imaging hybridization

The aim of surface functionalized with oligonucleotides and passivated with mercaptohexanol is to be applied as DNA chips. Therefore, oligonucleotides must be available for hybridization with a DNA strand of 1000 bases. In fact, after passivation with mercaptohexanol, oligonucleotides are well-dispersed on the surface. Hence, they acquire a configurational freedom which allows them to form double helix with complementary DNA strands. First, we have obtained two DNA single strands (DNAss) by the retro transcription of a messenger RNA (ARNm) selected for its biological interest. One of these strands being complementary to the oligonucleotide of 25 bases that we have grafted on the gold surface, our aim is to control the selectivity of our oligonucleotide functionalized surface. In order to verify AFM imaging results, we have also radio-labeled with P32 during the retro transcription process.

Once the DNAss is hybridized, the 25 bases of the molecule reacting with the oligonucleotide lead to a double strand which is quite stiff. In comparison, the free part of the DNAss appears like a linear chain of oligonucleotide, which diameter is smaller than the double strand. Hence, this free part is very flexible and can undergo important deformations. That is why it is often represented by a Gaussian polymer (Zhang Y., 2001), meaning that each monomer can be considered as a vector randomly oriented, considering electrostatic repulsion interactions between phosphate groups and pairing between complementary bases. In addition, as hybridization is carried out in a salt buffer, pairing between bases from the same strand can occur, facilitated by presence of counter ions, which neutralize phosphate groups charges (Montanari & Mézard, 2000).

The aim of AFM imaging is to differentiate non-hybridized oligonucleotides to hybridized ones from the different of size. Indeed, we have observed features of 2.5 nm height on hybridized surface (figure 6a), that we attribute to hybridized DNAss. The hybridization is confirmed by radioactivity scanning of a 1 cm^2 surface (figure 6c). In contrast, AFM image of hybridization with a non-complementary DNAss gives a low physisorption (figure 6b), which is confirmed by radioactivity scanning (figure 6d). However, the amount of hybridized molecules counted in AFM images is lower than radioactivity measures. This is probably due to the mobility of certain molecules chains, which renders them hard to observe with AFM.

In addition, some of the features of a “non-hybridized“ surface can be attributed to proteins contained in hybridization buffer. Indeed, the mercaptohexanol film makes the surface

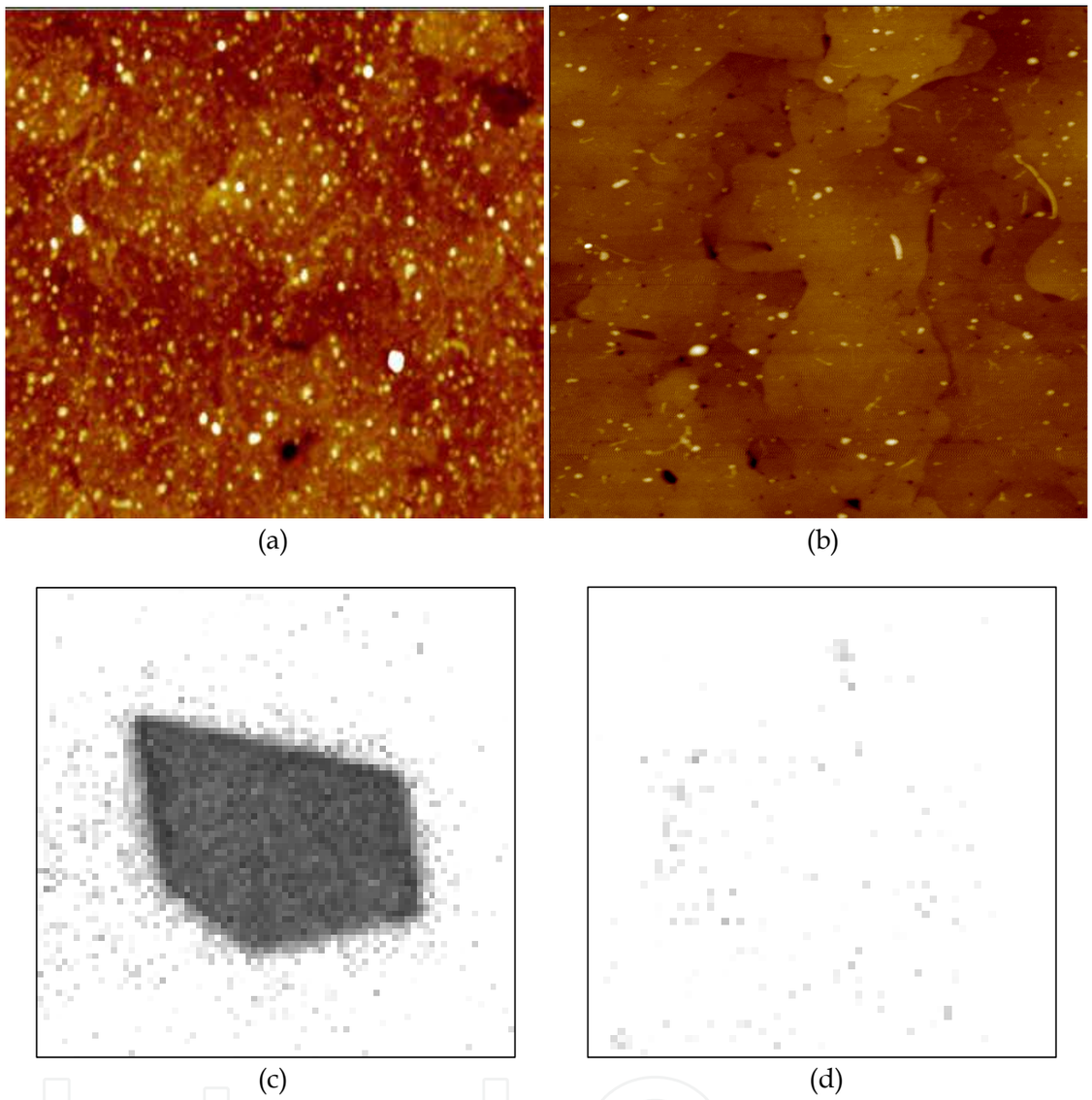

Fig. 6. Imaging of hybridization on surfaces functionalized with oligonucleotides and passivated with mercaptohexanol: With complementary DNAss : the amount of hybridized molecules evaluated 6a) on AFM image is of 10^3 molecules μm^{-2} and 6c) by radioactivity measurements (surface size of 1 cm^2) is of 5.10^3 molecules μm^{-2}. The size of AFM images is 1 μm × 1 μm and z scale is 7 nm; With non-complementary DNAss : the amount of hybridized molecules evaluated 6b) on AFM image is of 50 molecules μm^{-2} and 6d) by radioactivity measurement (surface size of 1 cm^2) is of 10 molecules μm^{-2}. The size of AFM images is 1 μm × 1 μm and z scale is 7 nm.

hydrophilic due to OH "end groups" present on the surface. Hence, proteins and DNA chains can adsorb on it. Without hybridization, non-complementary DNAss and protein are in competition. Whereas in presence of complementary DNAss, the reaction of hybridization is promoted. Moreover, their chains can be mobile on the surface with low electrostatic interactions with OH, hence becoming less visible to AFM.

In conclusion, AFM tapping mode permits one to image mechanism of passivation with SAM. According to hydrophobity or hydrophilicity properties of the SAM, interactions with molecules present on the surface vary. The hydrophilic SAM appears to let on the surface only the oligonucleotides which are well-chemisorbed and available for reactions. Furthermore, the differentiation between hybridized and non-hybridized oligonucleotides is successfully achieved by tapping mode thanks to size difference. Thus, AFM imaging becomes an alternative way of detecting directly reactions on surface, with the advantage of avoiding the preparation of labeled molecules.

5. Imaging 2D polymerized film

Functionalization with alkylsilane to form 2D polymerized film is of great interest in various fields, such as biosensors (Battistel et al., 1991; Schierbaum, 1994), microelectronics (Kumar et al., 1994; Burtman et al., 1999), catalysis (Juvaste et al., 1999; Yang et al., 2003), etc. For this purpose, alkylsilanes are grafted on glass (Ulman, 1991), silicon (Vandenberg et al., 1991; Kallury et al., 1994; Vrancken et al., 1995; Horr & Arora, 1997; Ek et al., 2003; Zhang & Srinivasan, 2004) or mica (Bezanilla et al., 1995; Lyubchenko et al., 1996; Tätte et al., 2003; Diez-Perez, 2004; Crampton et al., 2005, 2006) surfaces. Generally, it is assumed that molecules adsorb in an ordered film on the surface. Alkyloxy moieties form Si-O covalent bonds between the molecules or with the surface hydroxyl groups to build up a polymeric film anchored on the surface. In the case of bi-functionalized molecules, with a terminal group R such as H_2N^-, HO^-, HS^-, HSO_3^-, Cl^-, and Br^-, the second functionality R is expected to extend from the surface. However, often, more disordered monolayers are observed (Vandenberg et al., 1991; Kallury et al., 1994; Vrancken et al., 1995; Horr & Arora, 1997). Indeed, usually, both terminal groups are able to interact with the surface through hydrogen or electrostatic bonds, resulting in various configurations (Heiney et al., 2000; White & Tripp, 2000). Furthermore, because interactions between the molecules and the surface depend drastically on the substrate properties, a lack of reproducibility in film formation is often observed.

We have been interested by the functionalization of mica for reasons described above. Our molecule of interest for the formation of a 2D polymerized film is an aminosilane: *N*-(2-aminoethyl)-3 aminopropyltrimethoxysilane (AAPS). The adsorption of AAPS was studied on silica, and authors described it as an ordered film anchored on the surface via Si-O covalent bond, the amine functions extending from the surface (Chrisey et al., 1996; Ek et al., 2004). However, no experiment confirming this scheme was reported for AAPS on mica. In general, two ways of immobilizing a film on a surface exist: aqueous and vapor deposition.

5.1 Preparation of the substrate

In contrast to silica, freshly cleaved mica lacks native hydroxyl groups (Crampton et al., 2006), so covalent binding essential for the formation of a well-anchored layer of molecules seems unlikely. This problem is overcome by activating the surface through hydration to open up the silicate bonds (Kim et al., 2002). Two methods of hydration are possible:

- The first method consists of exposing the sample to a jet of steam (Schwartz et al., 1992). Figure 7 shows the evolution of the surface with time of exposition. After 30s of

exposure, surface presents 3-5 Å depth holes (figure 7a) and longer exposure, such as 90 s, leads to more or less wide 2D islands with a height of 1 nm (figure 7b). Because this height corresponds to the thickness of one mica leaflet, we attribute these islands to remaining pieces of the outer leaflet of mica, probably after a corrosion of the surface. Because an additional molecule layer also has a height on the order of 1 nm, this kind of surface is obviously not suitable for our study. Unfortunately, steam treatment of mica is not reproducible enough to obtain a surface without such islands.

- The second method of hydration consists of incubating the sample in water at room temperature. After 10 min of incubation, the AFM image shows a flat surface with no islands (figure 7c). In addition, this treatment leads to reproducible hydrated surfaces.

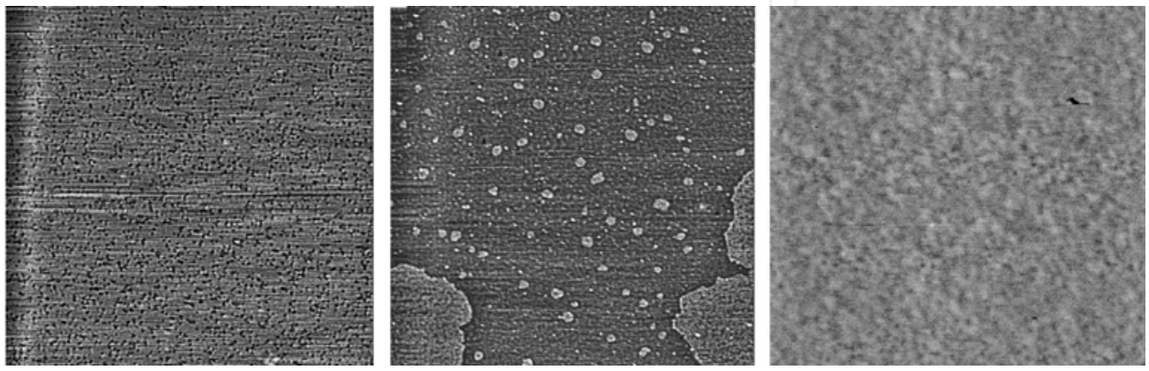

(a) (b) (c)

Fig. 7. AFM images (2 µm × 2 µm size) of the mica surface: 7a) exposed to a jet of steam for 30 s: holes correspond to a depth of 3-5 Å; 7b) exposed to a jet of steam for 90 s: islands correspond to a height of 1 nm; 7c) incubated in water for 10 min: holes correspond to a depth of 3-5 Å.

Finally, the chemical modifications due to both surface treatments are assessed by contact angle measurements. These are done immediately after completion of the treatment. Freshly cleaved mica shows a highly hydrophilic surface with a contact angle smaller than 5° (Seah & Dench, 1979). Incubation in water for 10 min makes it change to 20°. In the case of steam treatment, the contact angle measured on surfaces without islands increases with the time of exposure, also reaching 20°. This small variation in contact angle suggests that the surface is likely to be homogeneous. Thus, both methods similarly modify wetting properties of the surface. Even if we have no indication of the presence or the number of hydroxyl groups on the surface, we observe a lack of AAPS adsorption during the treatment in the vapor phase on a freshly cleaved mica surface.

For the adsorption in the aqueous phase, the molecule film depends neither on the previous hydration nor on the hydration method. This indicates that during the incubation in the solution of AAPS, the surface would be modified just like during incubation in water. Therefore, we have chosen the relevant hydration method depending on whether the subsequent molecule layer is performed through vapor or aqueous deposition. For vapor phase deposition of AAPS, mica is first hydrated by a jet of steam after precautious checking of the quality of the surface by AFM. For aqueous phase deposition, we routinely use the incubation method without checking the surface prior to molecules deposition.

5.2 Deposition in aqueous phase

In aqueous phase, the two amines contained by AAPS molecules can be either protonated or not, according to the solution pH. The mica lattice contains negative binding sites associated with Al and filled with potassium ions, K^+. In fluid, these cations (K^+) can be removed or displaced, as shown by surface force apparatus and XPS, presenting a negative surface potential (Crampton et al., 2005). For instance, protonated AAPS molecules (due to pH) can replace potassium ions, so they can adsorb preferentially on the surface. Therefore, pH must play a decisive role in the adsorption of AAPS on mica. For instance pure water (pH around 6) used to rinse the surface after immersion in AAPS solution, can protonate molecules. However, we have shown with XPS that for low concentrations, the number of molecules left after drying the surface without rinsing can be negligible.

5.2.1 Effect of pH

Experiments carried out by varying pH have allowed us to relate the protonation of AAPS amines to a $pK_{1/2}$ like the one introduced by Holmes-Farley et al. (Holmes-Farley et al, 1988). They defined the $pK_{1/2}$ for a liquid-solid interface as the value of the pH of the solution at which the functional groups at the interface are half-ionized. Thus, we have evaluated a $pK_{1/2}$ of 10-11 for the AAPS-mica interface, explaining the adsorption of AAPS by electrostatic interactions via protonated terminal amines only for pH's under 10 (Mourougou-Candoni & Thibaudau, 2009). In addition, the maximum surface density reached by protonated AAPS molecules is around 40% of the compact monolayer density. In fact, mica displays a large negative surface charge density in solution, which can form electrostatic bonds with protonated amine groups of aminosilane (Trens et al., 1995). Thus, we can relate the density of the protonated AAPS (i.e., 1.7×10^{14} molecules.cm^{-2}) to the density of negative charges on the bare surface, which is on the order of 1.8×10^{14} cm^{-2} (Maslova et al., 2004). Thus, our results clearly indicate that adsorption first proceeds by ionic interaction between the protonated amino groups and the negative charges of the surface until these are neutralized. Then electrostatic repulsion between protonated AAPS prevents their additional adsorption. Subsequently, only neutral molecules (with two free amines) are able to adsorb onto the surface.

5.2.2 Effect of incubation time

Exploring incubation time, we have evaluated that the density of molecule reach rapidly around 50% of the compact monolayer density and saturates at this value obtained by XPS measurements. Therefore, we investigate the configuration of AAPS molecules with AFM imaging in tapping mode (figure 8). We suppose that molecules cover either half of the surface, being upright on it, or the whole surface more or less lying flat on it. For 5 min of exposure, the substrate displays a homogeneous surface with a low roughness in the order of few angstroms (figure 8a); no island or structure of 1 nm height (corresponding to AAPS height) can be seen on the AFM image. Thus, it is clear that these AFM data are more in agreement with molecules lying flat on the surface. For longer exposure, bumps of heterogeneous heights around 0.5-1 nm appear on the layer (figure 8b). These bumps may correspond to small aggregates of upright molecules that are condensed on the surface or that have been already formed in the solution. However, we have not observed the formation of a structured layer of molecules leading to a film of molecules on the surface.

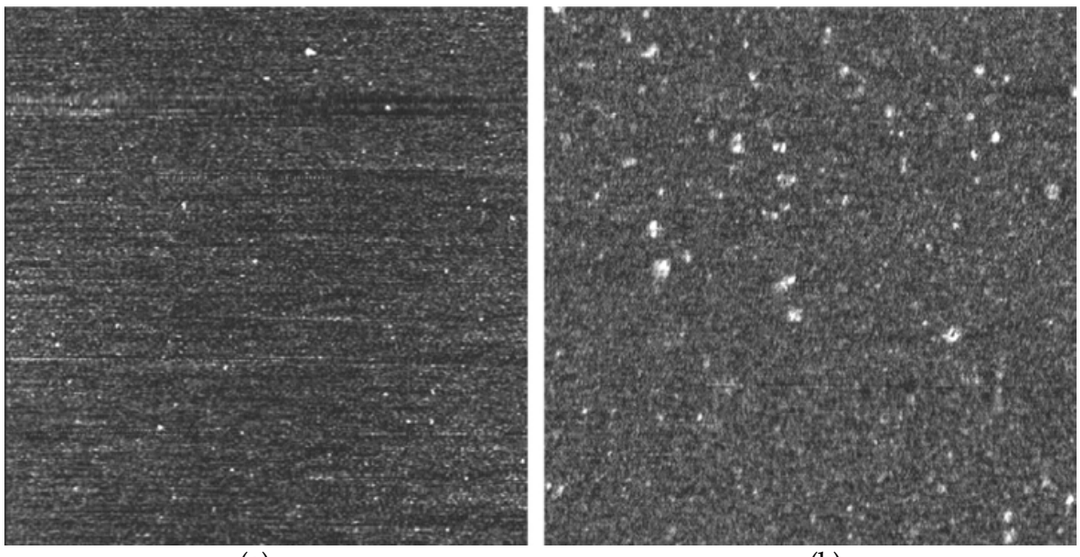

(a) (b)

Fig. 8. AFM images (2 μm × 2 μm size) of hydrated mica surface incubated in a solution of AAPS at 40 μM for (8a) 5 min and (8b) 45 min. The darker to brighter features correspond to 1 nm height.

Although AAPS adsorption in aqueous phase gives interesting results concerning the dependence with pH, we note limitations due to film disordering on the surface and copolymerization of AAPS in the liquid. It must be pointed out that this kind of problems may happen with every alkyloxy molecule because they can polymerize in solution. We insist on the importance of these experiences because they demonstrate clearly that surface analysis techniques must be completed by a direct visualization via AFM in order to study film formation.

5.3 Deposition in vapor phase

5.3.1 Formation of monolayer

To overcome problems of self-polymerization, deposition in the vapor phase can be also proposed because molecular density is lower in the vapor phase. Indeed, self-assembled monolayers have been obtained with silane on silicon (Sugimara et al., 2002). In our experiments, the mica surface is exposed to AAPS vapor under an anhydrous nitrogen atmosphere at room temperature for 15 min to 48 h, and afterward, the surface is imaged by AFM (figures 9). For 15 min of exposure to AAPS, the surface appears rough with few bi-dimensional islands (figure 9a). These islands and the surrounded surface heights are of 0.8 and 0.4-0.5 nm, respectively. This must be compared to the roughness of 0.2 nm of the mica substrate before its exposure to AAPS. After 1 h of exposure, figure 9b shows a quite homogeneous film with holes of 0.8 nm depth (with few bumps).

In addition, the contact angle of a water drop on the surface increases with exposure time, reaching ~50° on the film. This value is in the range of contact angles reported for aminosilanes films (40-63°) (Song et al., 2006). Moreover, because the length of AAPS molecules is on the order of 1 nm, islands are probably formed by condensed upright AAPS

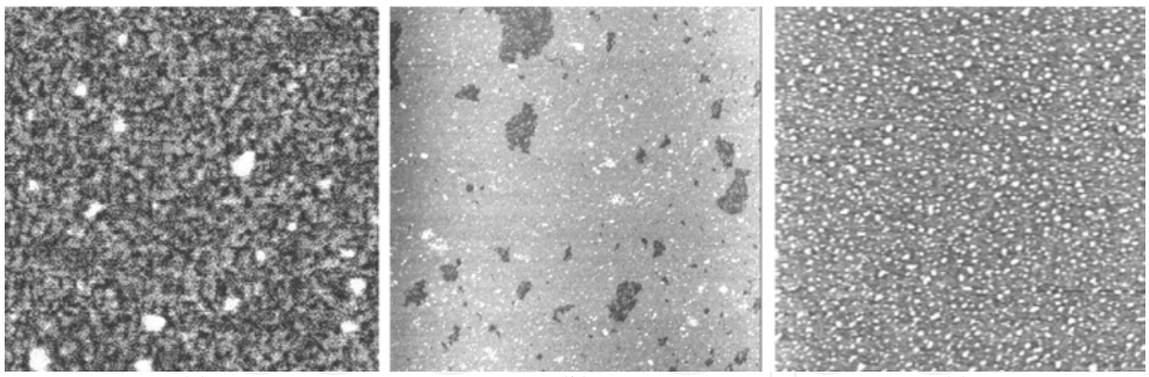

(a) (b) (c)

Fig. 9. AFM images of hydrated mica surfaces exposed to vapor of AAPS under anhydrous nitrogen atmosphere: 9a) For 15 min (1 µm × 1 µm size) the darker to brighter features correspond to 1 nm height; 9b) For 1 h (2 µm × 2 µm size), light gray to dark gray features correspond to 1 nm height; 9c) For 48 h (2 µm × 2 µm size), dark gray to white features correspond to 10 nm height.

molecules (0.8 nm), which are surrounded by prone molecules (0.4-0.5 nm). The film obtained after 1 h of exposure is undoubtedly a monolayer of upright molecules on the surface. According to these results, we infer that molecules first adsorb onto the surface in a disordered phase, and then they condense into islands, which grow and coalesce to form a monolayer.

5.3.2 Restructuration of layers

For a longer treatment (48h), AFM images show that the surface increases in roughness, with bumps of ~2-4 nm height (figure 9c). Hence, after the first monolayer has grown, adsorbed molecules instead form 3D clusters. This phenomenon is similar to the well-known Stransky-Krastanov crystalline growth mode. This mode appears when the interfacial energy between the surface and the first monolayer is lower than the surface energy of the monolayer and when the interfacial energy between the first monolayer and successive layers is higher than the surface energy of successive layers. Actually, this structure is not stable and changes with exposure to ambient atmosphere. Indeed, the surface morphology of the sample presented in figure 9c is obviously modified after 24 h in ambient atmosphere (figure 10a): it is covered with numerous small, bi-dimensional islands of 1.7 nm height and a few larger islands. However, "pinholes" of 0.8 nm depth on the film supporting the islands (figure 10b) indicate that the first monolayer does not drastically change and that the restructuring instead concerns the matter on it. The depletion area surrounding the highest islands (figure 10a) indicates that they grow from the surrounding matter. This is typical of a dewetting phenomenon.

According to this reorganization, it is obvious that molecules are mobile prior to exposure to the ambient atmosphere. The more realistic assumption to explain this mobility is that polymerization is not complete after exposure to AAPS under anhydrous nitrogen atmosphere, certainly due to the lack of water molecules for the hydrolysis of the methoxy ends, whereas when the surface shown in figure 9c is exposed to ambient humidity, hydrolysis

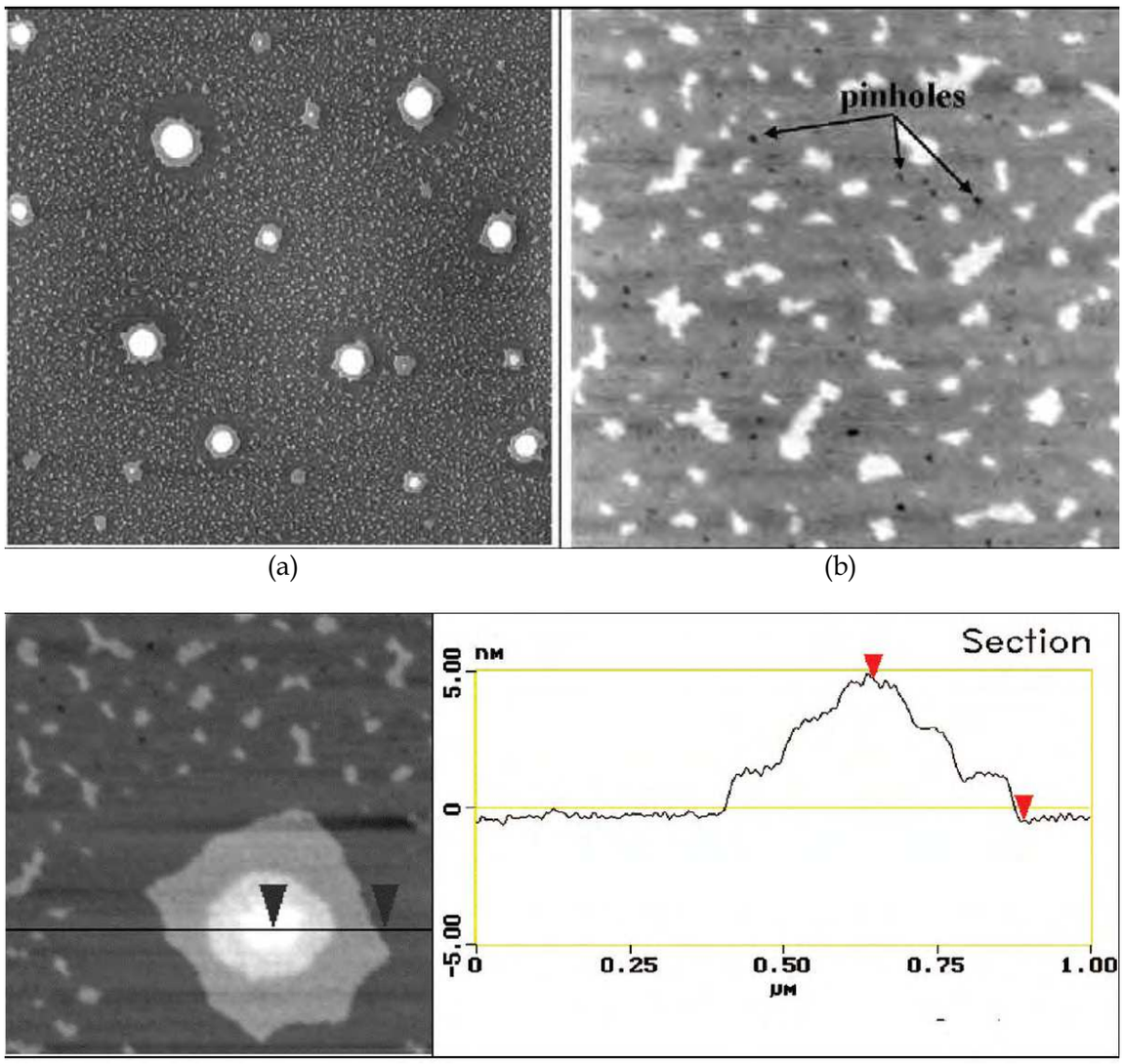

Fig. 10. AFM images of mica surface treated for 48 h to vapor of AAPS and exposed 24 h in ambient atmosphere at room temperature: 10a) The size of the image is of 10 µm × 10 µm, the darker to brighter features correspond to 15 nm height; 10b) Magnified image (2 µm × 2 µm size) of bilayer islands with pinholes of 0.8 nm depth on the film supporting the bilayer islands; 10c) Magnified image (1 µm × 1 µm size) of a high island with superposed bilayers; 10d) Section analysis of the high island of panel 10c.

occurs, which triggers polymerization and film reconstruction. Concerning the larger islands, some of them are of 1.7 nm height, but most display one or more stacked bi-dimensional islands of 1.7 nm height like a set of "Russian dolls". For example, figure 10c shows a large island composed of three stacked bi-dimensional islands of 1.7 nm height (see cross section in figure 10d). Such a stacking indicates an order in the film above the first monolayer, perpendicular to the surface. The quantification of heights measured with AFM (of 0.8 nm for the first monolayer and 1.7 nm for islands) clearly rules out a non-structured film.

5.3.3 Configuration of molecules

This study with AFM imaging and contact angle measurements allows us to deduce a schematic for the formation of AAPS layers on mica. For the first monolayer, a contact angle of ~60° is expected for the 100% amino-terminated monolayer (N. P. Huang et al., 2001). In our case (50°), we clearly obtain a uniform assembly of upright molecules with amine ends oriented mainly outward. In addition, this monolayer does not change from exposure under anhydrous atmosphere to ambient atmosphere (figure 10b). This obviously means that molecules interact among themselves or with the surface when they adsorb under anhydrous atmosphere. However, Si-O covalent bonds must be rare due to the lack of water molecules for the hydrolysis of the methoxy ends. Therefore, molecules are probably self-assembled on the surface via van der Waals interactions.

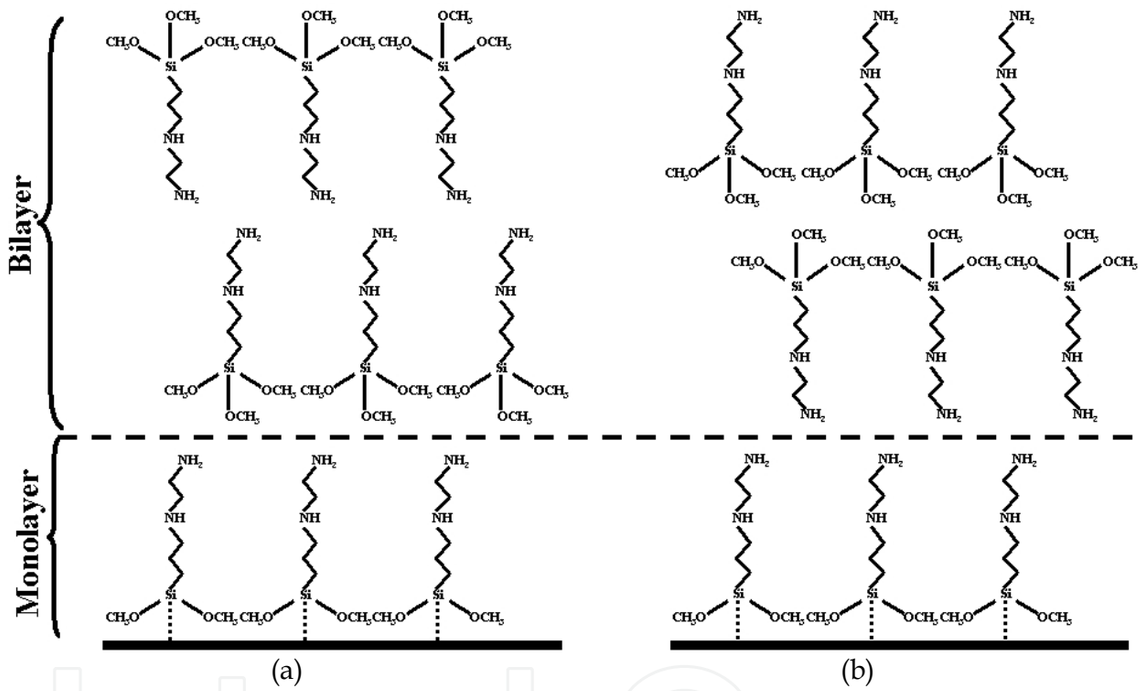

Fig. 11. Possible configurations of the bilayer: molecules in the bilayer are standing either head-to-head or tail-to-tail. (The first monolayer is a self-assembly of upright molecules with amine ends mainly oriented outward.)

For the film above the first monolayer, exposure to ambient atmosphere restructures it in bi-dimensional islands with a perpendicular periodicity of 1.7 nm, which is approximately twice the height of a monolayer. This suggests that islands are formed of one bilayer of upright molecules. If molecules in the bilayer were arranged head to tail, we would also observe a stacking periodicity of 0.8 nm order perpendicular to the surface. Consequently, molecules are standing either head-to-head, or tail-to-tail. According to these remarks, only two (coarse) orientations are possible for AAPS molecules of the film superposed to the first monolayer (figure 11a and b). Moieties displayed at the interface with air are methoxy ends in figure 11a and amine ends in figure 11b. Therefore, contact angle measurements on the bilayer could discriminate between both configurations, but these measurements are quite

imprecise, probably due to the mobility of the bilayer. However, if the interaction between a tail and a head is preferential in the interface between the first monolayer and the subsequent film, as in the configuration of figure 9a, then it is also the case inside the bilayer. Therefore configuration 11a is not self-consistent, contrary to configuration 11b.

More precisely, molecules oriented as in figure 11b can display two structures. The first one, hereafter called a double leaflet structure, consists of two superposed leaflets with structure and density similar to the first monolayer, molecules of a leaflet polymerizing with each other (figure 12a). The second structure, hereafter called a single-leaflet structure, consists of only one sheet of 2D polymerized molecules, the tails of these molecules being alternatively localized on each side of the polymerization plan (figure 12b). In this case, the density of tails on each side of the polymerization plan is half of that in the first layer, and we can expect that the tails of molecules are tilted to pack the structure. Of the two structures, the latter seems more realistic to us if we consider their formation. In fact, the double-leaflet structure, figure 12a, implies that molecules of the leaflet close to the monolayer (inner leaflet) must be completely polymerized before the other leaflet (outer leaflet) extends on it. Otherwise a cross-polymerization will occur between both leaflets, and in the limiting case, it will lead to the single-leaflet structure. Therefore, if the double-leaflet structure is valid, we will observe areas with the inner leaflet covered partially by the outer leaflet.

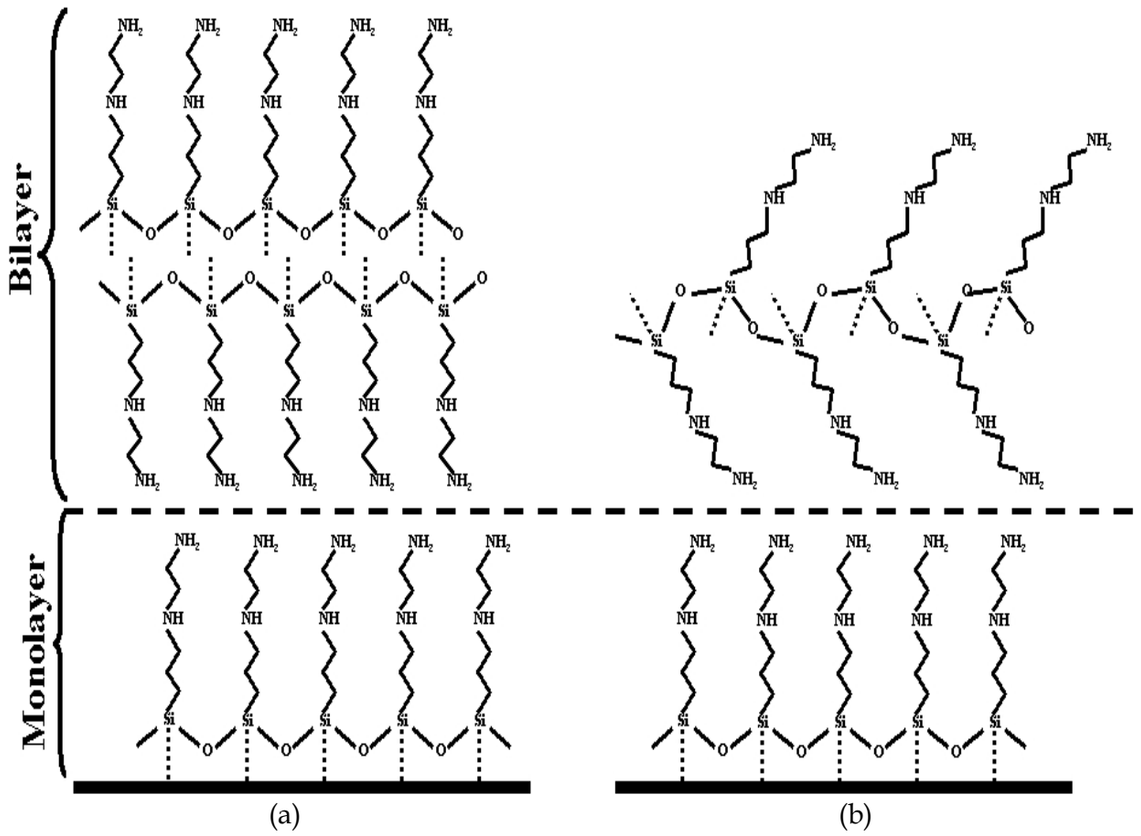

Fig. 12. Possible structures of AAPS bilayers: 12a) the double-leaflet structure, two superposed leaflets with molecules of a leaflet polymerizing with each other; 12b) the single-leaflet structure, one sheet of 2D polymerized molecules.

In addition, the dewetting behavior observed on AFM images in ambient atmosphere is driven by a difference between interfacial energies. In fact, the interfacial energy between the first monolayer and the bilayer must be different from the interfacial energy between bilayers. In the case of the double-leaflet structure, both interfaces are similar, given by the chemistry and the density of tails, which are the same in the monolayer and in the bilayer. In contrast, in the single leaflet structure, the density of tails at interfaces between bilayers is different from the one at the interface between the first monolayer and the bilayer. This undoubtedly leads to different interfacial energies. Thus, the single-leaflet structure correlates with the behavior of bilayers. On the basis of energy considerations or formation mechanisms, configuration 12b seems to be the most realistic structure. In order to determine precisely the organization of the molecules in the bilayer, we have to reach a molecular resolution on these films with AFM.

In conclusion, AFM imaging allows us to study the formation and structure of AAPS on mica thanks to a systematic study of deposition conditions and their effects. It must be pointed out that this kind of exploration must be undertaken to understand functionalization of surface with 2D polymerized films. Thus, in aqueous treatment the interaction of molecules with the surface depends on the pH, as compared to the $pK_{1/2}$ that must be evaluated through AFM imaging and surface analysis techniques. In this work, only for pH's under 10 does the AAPS adsorb on the mica surface by electrostatic interactions via protonated terminal amines and no formation of a structured layer of molecules is observed. Therefore, tapping mode has been used to thoroughly investigate vapor treatment, demonstrating that the film of AAPS is composed of a first monolayer and successive bilayers. We must point out that AFM imaging has lead to the first observation of such an organization in aminosiloxane films, to our knowledge.

6. Development on conventional AFM in tapping mode

We have presented in the parts above various potentialities of conventional AFM in tapping mode for imaging functionalized surfaces. We have based our argumentation on experiments carried out on very different ways of functionalization, such as aqueous or vapor treatments leading to isolated single molecules, SAMs or polymer 2D films. However, parameters such as resolution, environment and speed of imaging must be improved according to the functionalizing process. Therefore, many developments on conventional AFM tapping mode have been carried out contributing to its imaging capacities and its applications.

6.1 Topographic imaging resolution

The first application of AFM in tapping mode is topographical imaging. In this field, the principal requirement is the resolution.

6.1.1 Improvements in tip development

In conventional AFM in tapping mode, we have mentioned that the radius of curvature of the tip and its shape are of great importance for the imaging resolution in air. In addition, the surface chemistry of the tips, usually not well defined, may limit the application of tapping AFM in the investigation of functionalized surfaces. A great breakthrough in terms

of resolution comes from carbon nanotubes attached to the end of the tip (figure 13) (Dai et al, 1996; Hafner et al., 2001; Wong et al., 1998a, 1998b). Indeed, carbon nanotube tips possess a high aspect ratio, mechanical robustness, small diameter and a well-defined surface chemistry. The resolution attainable with these tips is comparable with that of other ultimate resolution imaging techniques such as cryogenic electron-microscopy (Koehne, 2011; Kitazawa, 2011). In addition, nanotubes also offer the possibility to be functionalized, exposing, thus, well-defined chemical groups or chemisorbed biomolecules. This opportunity can be exploited to study the spatial distribution of chemical functional groups or complementary biomolecules as for hybridization (Woolley, 2004).

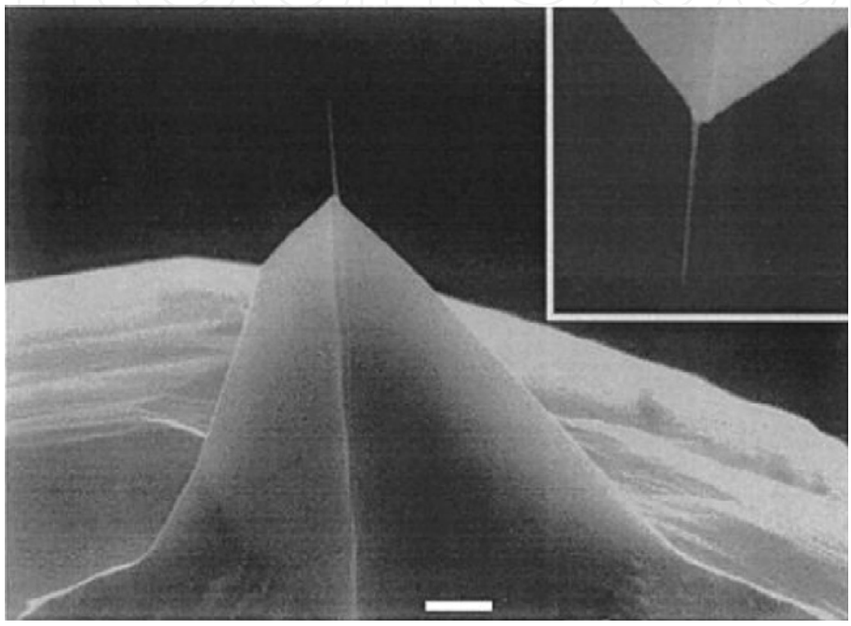

Fig. 13. Carbon nanotube attached to the end of a silicon tip. The inset is a higher magnification view of the same tip rotated 180°◦ relative to the main image (bar = 1 μm) (Alessandrini & Facci, 2005).

6.1.2 Improvement in force control

Resolution can also be improved by accurately controlling the interaction between tip and sample. The variation of the tip-sample force is achieved by changing the amplitude of the freely oscillating tip called driving amplitude, DA, and the set-point amplitude, SP. The effective tip-sample force increases with DA and/or the difference (DA-SP) (Höper et al., 1995) by modifying the set point, which balances the contribution of attractive and repulsive forces. (San Paulo & Garcia, 2000). Thus, an automatically adjusted set-point can produce lower force measurements at higher spatial resolutions (Möller et al., 1999). However, in imaging in air, an attractive force appears due to the layer of water condensation and other contamination which often covers both tip and sample. Indeed, water forms a meniscus pulling the tip and sample together. The resulting strong attractive force is usually of 10 to 100nN, making high-resolution imaging difficult and sometimes causing sample damage. (Dufrêne, 2002). These capillary forces can be eliminated by performing the imaging in aqueous solution, and so maximizing resolution (Alessandrini & Facci, 2005).

6.2 Non-topographical modes of imaging

In contrast to the contact mode, the height images of the tapping mode can show minor, and sometimes, barely detectable variations with changes in the force. In this case, the frequency and phase of the oscillating cantilever are more sensitive to the tip-sample interaction force.

6.2.1 Frequency imaging

The description of the vibrating probe as a harmonic oscillator shows that repulsive tip-sample force interactions cause a shift of the resonant frequency to high frequencies and related phase changes (Dürig et al., 1992). Attractive forces decrease the resonant frequency. The images of frequency shifts provide new information about surface topography and other properties (Babcock et al., 1995). The frequency shift images are not widely used in measurements at ambient conditions because the low Q-factor of the cantilever in air makes it difficult to track the small negative frequency shifts and to use them for the feedback required for imaging in the attractive force regime (Magonov et al.,1997a). Such an operation works well in ultra high vacuum (UHV) where the Q-factor of the oscillating probe is extremely high. Hence, atomic-scale defects of several semiconductor lattices were observed in this mode (Sugawara et al., 1995).

6.2.2 Phase imaging

In tapping AFM, the phase images are often recorded simultaneously with the height images. They show the variations, at different points on the surface, of the phase of the oscillating tip determined at the fundamental resonant frequency of the freely oscillating tip. Therefore, phase of the tip is adjusted to zero before the tip engages the sample. Phase images provide the best contrast of fine morphological and nano-structural features due to their high sensitivity to surface imperfections such as steps, cracks, and the like. On surfaces with local variations of mechanical properties, the phase changes are even more informative (Magonov et al., 1997b). The phase shift being strictly related to the amount of energy dissipated in the tip–sample contact, mapping the phase shift permits to identify regions of different interaction properties (Cleveland et al., 1998, Tamayo & Garcia, 1997). For instance, gold nanoparticles adsorbed on a phospholipidic bilayer functionalizing a surface of mica give topographical images showing gold nanoparticles with blurred outline (figure 14a). In contrast, phase images clearly permits to distinguish gold nanoparticles with well-defined outline (figure 14b). Thus, the stiffness-related contrast of the phase images offers new possibilities for imaging multi-component samples.

6.3 Imaging resolution in liquid

The development of tapping AFM mode in liquid configured an important breakthrough for the application of the AFM in the case of single molecules or films, which are loosely immobilized. Applications of this method concerns also many other objects, like biological materials, which must be observed in their native environment, thereby opening the possibility of analyzing their structural and functional aspects at the sub-molecular level (Kumar et al., 2005). By selecting appropriate buffer conditions, it is generally possible to maintain an applied force in the range of 0.1 to 0.5 nN. Therefore, a preliminary investigation is recommended on pH and ionic strength effects on the image quality in order

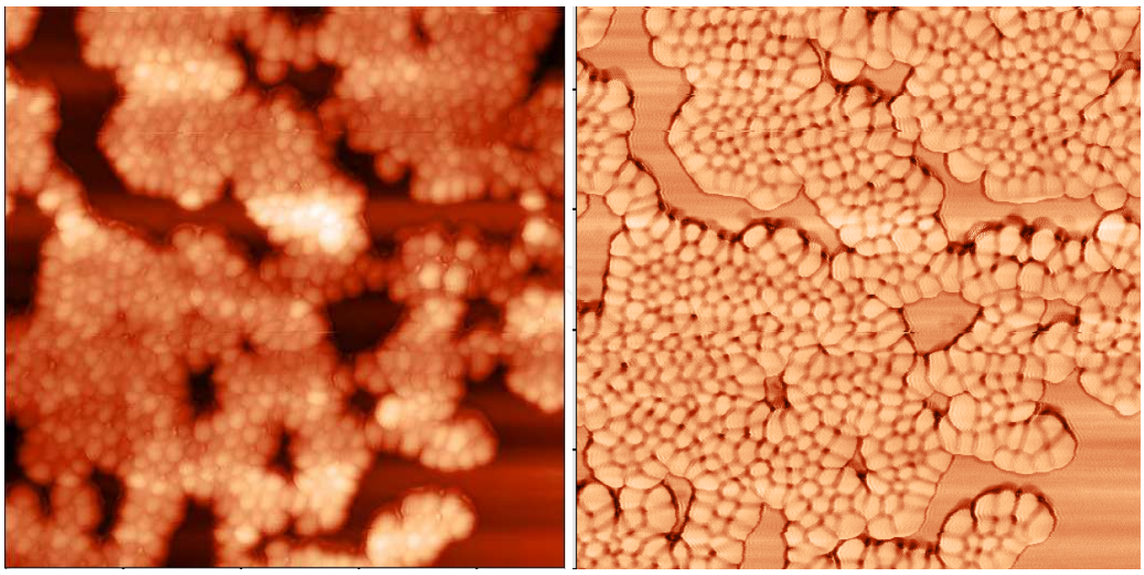

(a) (b)

Fig. 14. AFM images of gold nanoparticles adsorbed on a phospholipidic bilayer functionalizing a surface of mica, the size of AFM images is 0.5 µm × 0.5 µm and z scale is 50 nm: 14a) the topographical image shows gold nanoparticles with blurred outline. 14b) the phase image shows nanoparticles with well-defined outline.

to define an optimal imaging environment. Also, because of thermal drift, it is often essential to readjust the applied force between image acquisitions.

For measurements, the sample is immersed in the buffer, in a cell which can be thermostatted, permitting diffusion of molecules and phase transitions of films. An example of the phase transition of a phospholipidic single-bilayer supported on a mica substrate is shown in figure 15 by real time temperature controlled atomic force microscopy. Authors distinguish two-phase transitions in this bilayer arising from the independent melting of each leaflet at different temperatures (Charrier & Thibaudau, 2005). They observe shifts in temperature that they attribute to different leaflet compressions induced by the adsorption of the lipids on the mica substrate. Such studies on fluidity of phospholipid films are a major feature required for technological applications. Indeed because phospholipid bilayers are highly electrically resistant, and ordered, they can be used for biosensor technologies based on electrical and optical detections (Dumas et al., 2011).

However, a fundamental drawback of working in liquid is the reduction of the *Q* factor of the cantilever. This reduction is caused by the viscosity of the surrounding liquid. The relative high *Q* value observed in air ensures a high sensitivity since a small shift in the resonance frequency, caused by tip-sample interaction, produces a large drop in the amplitude of the oscillation. In liquids, as the resonance peak is much broader, a small shift in the resonance frequency induces a moderate change in the amplitude of oscillation (Moreno-Herrero et al., 2004). A better way to control the force applied by the tip is an active quality factor control (active-Q). This is a technique which permits to increase the otherwise low quality factor for the oscillating cantilever in liquid and correspondingly to decrease the force applied by the tip on the sample (Alessandrini & Facci, 2005; Tamayo et al., 2000, 2001).

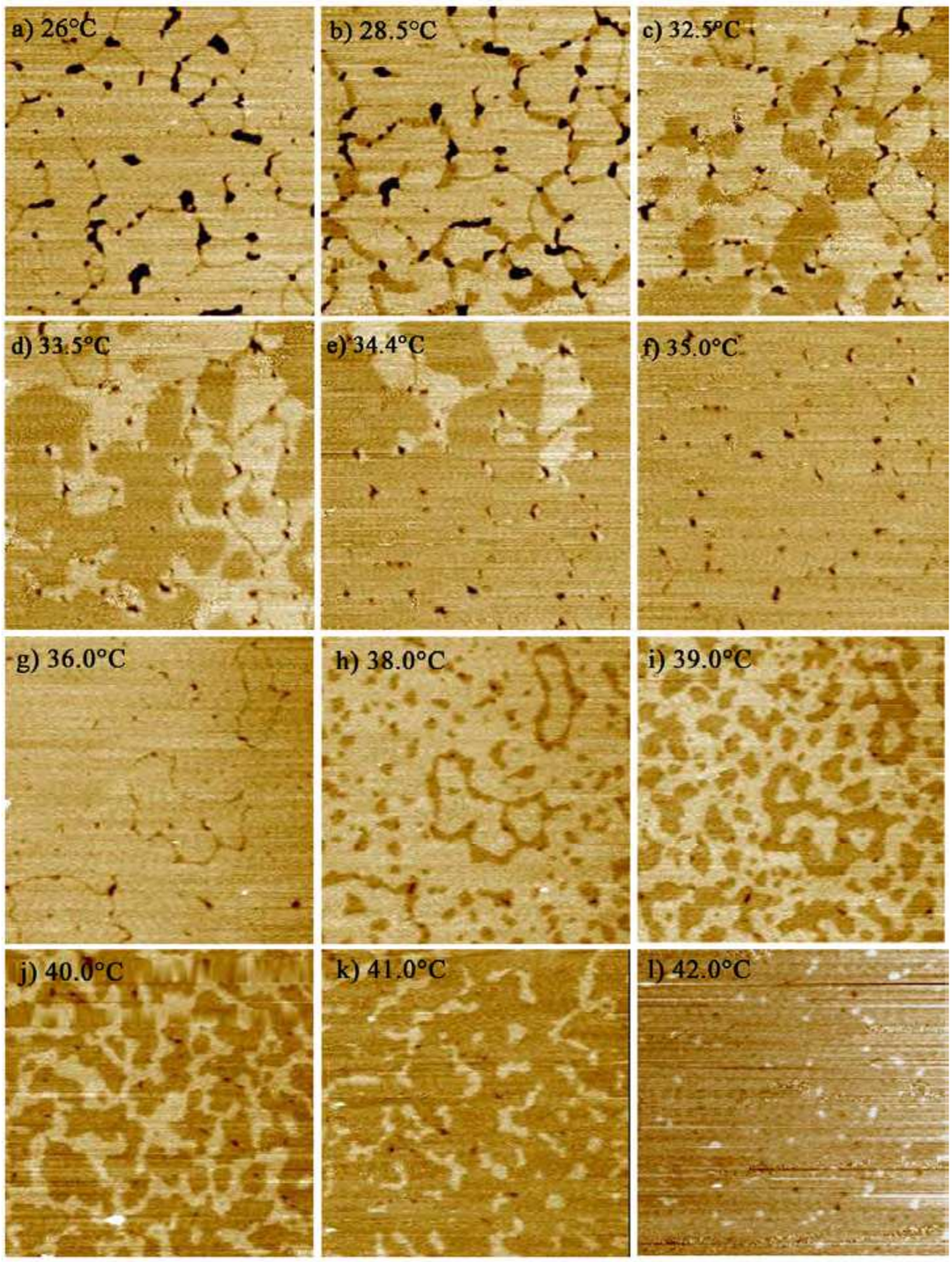

Fig. 15. AFM images (size 3 μm × 3 μm) of the transitions of a supported single-bilayer at different temperatures. The darkest areas are holes in the bilayer. The sample is continuously heated under the AFM tip at a rate of 0.1°C min^{-1}. The temperature indicated on each image corresponds to the temperature in the middle of the image (Charrier & Thibaudau, 2005).

6.4 Improvements on scanning speed

Increasing the scanning speed of AFM in tapping mode permits to follow dynamics of process on functionalized surface, at a nanometer scale. In fact, processes can occur on a millisecond timescale or less, while one image takes generally more than a minute to be captured. The scanning speed is limited by mechanical constraints (Butt et al., 1993). The dynamic of the piezoelectric scanner is a limit for high speed imaging. The dynamic is enhanced by using smaller high-frequency piezo segments to move z-scanner (Mamin et al., 1994; Zhao et al., 2011). Concerning the xy-scanner, an attempt to minimize coupling motions is carried out. Because the scanning speed of each direction may differ, the linear motion stage for a high-speed scanner is designed to have different resonance frequencies for the modes, with one dominant displacement in the desired directions. This unsymmetrical configuration separates the frequencies of two vibration modes with one dominant displacement in each desired direction, and hence suppresses the coupling between motions in two directions (Park & Moon, 2011). Another constraint is to maintain a high signal-to-noise ratio during high speed scanning. Therefore, cantilevers with higher resonant frequencies are needed, while their spring constant should remain constant. For instance, the mass of the cantilevers can be reduced, which permits to combine high resonance frequency with small spring. One way is to reduce the size of cantilevers (9-40 μm) leading to MHz resonance frequency (Walters et al., 1996). Thanks to these cantilevers, authors obtained a sequence of images in liquid at few ms intervals (Ando et al., 2001, Lyubchenko et al., 2011). The last but not the least limiting point is the time taken by the oscillating cantilever to change amplitude (Sulchek et al., 2000). This time can be reduced by implementing an active damping circuit (Sulchek et al., 2002; Fleming et al., 2010).

7. Acknowledgment

I would like to thank Pr. Franck Thibaudau, Dr. Cathy Naud, Dr. Isabelle Meunier and Mr. Jean-Matthieu Barbier for their participation in this work. Dr. Catherine Nguyen and Dr. Béatrice Loriot are thanked for their participation in preparation of biological materials and helpful discussions on DNA hybridization. Dr. Anne Charrier is gratefully thanked for producing comparative height and phase images, figure 14; and images of temperature dependent transitions in liquid AFM, figure 15.

8. References

Ando, T.; Kodera, N.; Takai, E.; Maruyama, D.; Saito, K. & Toda, A. (2001) A high-speed atomic force microscope for studying biological macromolecules, *Proc. Natl Acad. Sci. USA,* Vol. 98, pp. 12468–12472

Alessandrini, A. & Facci, P. (2005) AFM: a versatile tool in biophysics, *Meas. Sci. Technol.*, Vol. 16, pp. R65–R92

Aslam, M.; Bandyopadhyay, K.; Lakshminarayanan, V. & Vijayamohanan, K. (2001) *J. Colloid. Interface Sci.,* Vol. 234, pp. 410

Babcock, K.; Dugas, M.; Manalis, S. & Elings, V. (1995), *MRS Symp. Proc.,* Vol. 355, pp. 311

Bandyopadhyay, K.; Vijayamohanan, K.; Venkataramanan, M. & Pradeep, T. (1999) *Langmuir,* Vol. 15, pp. 5314

Battistel, E.; Bianchi, D. & Rialdi, G. (1991) *Pure Appl. Chem*., Vol. 63, pp. 1483

Bezanilla, M.; Manne, S.; Laney, D. E.; Lyubchenko, Y. L. & Hansma, H. G. (1995) *Langmuir*, Vol. 11, pp. 655–659

Binnig, G.; Quate, C.F. & Gerber, C. (1986) Atomic Force Microscope. *Phys. Rev. Lett*., Vol. 56, pp. 930–933

Burtman, V.; Zelichenok, A.; Yakimov, A. & Yitzchaik, S. (1999) In *Semiconducting Polymers: Applications, Properties and Synthesis*; American Chemical Society: Washington, DC, Chap. 25

Butt, H. J. ; Siedle, P. ; Seifert, K. ; Fendler, K. ; Seeger, T. ; Bamberg, E.; Weisenhorn, A. L. ; Goldie, K. & Engel, A. (1993) Scan speed limit in atomic force microscopy, *J. Microsc.*, Vol. 169, pp.75–84

Charrier, A & Thibaudau, F. (2005) Biophys. J., Vol. 89, pp. 1094–1101

Chrisey, L. A.; Lee, G. U. & O'Ferrall, C. E. (1996) *Nucleic Acids Res.*, Vol. 24, pp. 3031-3039

Cleveland, J. P.; Anczykowski, B.; Schmid, A. E. & Elings, V. B. (1998) Energy-dissipation in tapping-mode atomic-force microscopy, *Appl. Phys. Lett.,* Vol. 72, pp. 2613–2615

Cloarec, J. P.; Martin, J. R.; Polychronakos, C.; Lawrence, I.; Lawrence, M. F.; Souteyrand, E. (1999) *Sens. Actuators B*, Vol.58, pp. 394-398

Crampton, N.; Bonass, W. A.; Kirkham, J. & Thomson, N. (2005) *Langmuir*, Vol. 21, pp. 7884–7891

Crampton, N.; Bonass, W. A.; Kirkham, J. & Thomson, N. (2006) *Ultrmicroscopy*, Vol. *106*, pp. 765–770

Dai, H.; Hafner, J. H. & Lieber, C. M. (1996) Nanotubes as nanoprobes in scanning probe microscopy, *Nature*, Vol. 384, pp. 147–51

Diez-Perez, I.; Luna, M.; Teheran, F.; Ogletree, D. F.; Sanz, F. & Salmeron, M. (2004) *Langmuir*, Vol. 20, pp. 1284

Dubois, L. H. & Nuzzo, R. G. (1992) Synthesis, structure and properties of model organic surfaces, *Annu. Rev. Phys. Chem.,* Vol. 43, pp. 437–463

Dufêne, Y. F. (2002) Atomic Force Microscopy, a Powerful Tool in Microbiology, *Journal of bacteriology*, Vol. 184, No. 19, pp. 5205–5213

Dumas, C.; El Zein, R.; Dallaporta, H.; & Charrier, A. (2011), Autonomic Self-Healing Lipid Monolayer: A New Class of Ultra-Thin Dielectric, *Langmuir*, DOI. 10.1021/la202333n

Dürig, U.; Zuger, O. & Stadler, A. (1992) *J. Appl. Phys.,* Vol. 72, pp. 1778

Ek, S.; Iiskola, E. I.; Niinistï, L.; Vaittinen, J.; Pakkanen, T. T.; Keränen, J. & Auroux, A. (2003) *Langmuir*, Vol. *19*, pp. 10601-10609

Ek, S.; Iiskola, E. I. & Niinistö, L. (2004) *J. Phys. Chem. B*, Vol. 108, pp. 9650–9655

Estroff, L. A.; Kriebel, J. K.; Nuzzo, R. G. & Whitesides, G. M. (2005) Self-Assembled Monolayers of Thiolates on Metals as a Form of Nanotechnology, *Chem. Rev.*, Vol. 105, n°4, pp. 1103–1170

Fleming, A.J.; Aphale, S.S.; Moheimani, S.O.R. (2010) A New Method for Robust Damping and Tracking Control of Scanning Probe Microscope Positioning Stages, *IEEE Transactions on nanotechnology*, Vol. 9, N°4, pp. 438-448

Hafner, J. H.; Cheung, C-L.; Woolley, A. T.& Lieber, C. M. (2001) Structural and functional imaging with carbon nanotube AFM probes, *Prog. Biophys. Mol. Biol.,* Vol. 77, pp. 73–110

Hansma, H. G.; Revenko, I.; Kerry, K. & Laney, D. E. (1996) *Nucleic Acids Res.*, Vol. 24, No. 4, 713-720

Heiney, P. A.; Grüneberg, K.; Fang, J.; Dulcey, C. & Shashidhar, R. (2000) *Langmuir*, Vol. 6, pp. 2651

Herne, T. M. & Tarlov, M. J. (1997) *J. Am. Chem. Soc.*, Vol. 119, pp. 8916- 8920

Holmes-Farley, S. R.; Bain, C. D. & Whitesides, G. M. (1988) *Langmuir,* Vol. 4, pp. 921–937

Höper, R.; Gesang, T.; Possart, W.; Hennemann, O-D. & Boseck, S. (1995) *Ultramicroscopy,* Vol. 60, pp. 17

Horr, T. J. & Arora, P. S. (1997) *Colloid Surf., A,* Vol. 126, pp. 113

Huang, N. P.; Michel, R.; Voros, J.; Textor, M.; Hofer, R.; Rossi, A.; Elbert, D. L.; Hubbel, J. A. & Spencer, N. D. (2001) *Langmuir*, Vol. 17, pp. 489

Huang, E.; Satjapipat, M.; Han, S. & Zhou, F. (2001) *Langmuir* , Vol. 17, pp. 1215-1224

Jalili, N. & Laxminarayana, K. (2004) Mechatronics, Vol. 14, pp. 907–945

Juvaste, H.; Iiskola, E. I. & Pakkanen, T. T. (1999) *J. Organomet. Chem.,*Vol. 587, pp. 38

Kaifer, A. (2001) *Supramolecular Electrochemistry,* Coral Gables. Wiley VCH. pp. 191–193

Kallury, K. M. R.; Macdonald, P. M. & Thompson, M. (1994) *Langmuir , 10*, 492.

Kelley, S. O.; Barton, J. K.; Jackson, N. M.; McPherson, L. D.; Potter, A. B.; Spain, E. M.; Allen, M. J. and Hill, M. G. (1998) L*angmuir*, Vol. 14, No. 24, 6781-6784

Kim, S.; Christenson, H. K. & Curry, J. E. (2002) *Langmuir*, Vol. 18, pp. 2125–2129

Kitazawa, M. ; Ito, S.; Yagi, A.; Sakai, N.; Uekusa, Y.; Ohta, R.; Inaba, K.; Hayashi, A.; Hayashi, Y.; Tanemura, M. (2011) High-Resolution Imaging of Plasmid DNA in Liquids in Dynamic Mode Atomic Force Microscopy Using a Carbon Nanofiber Tip, *Japaneses journal of applied physics*, Vol. 50, N°8, special issue

Klein, H.; Blanc, W.; Pierrisnard, R. ; Fauquet, C. & Dumas, Ph. (2000) *Eur. Phys. J. B*, Vol. 14, pp. 371-376

Koehne, J. E.; Stevens, R. M.; Zink, T.; Deng, Z.; Chen, H.; Weng, I. C.; Liu, F. T. & Liu, G. Y. (2011) Using carbon nanotube probes for high-resolution three-dimensional imaging of cells, *Ultramicroscopy*, Vol. 111, N°8, pp.1155-62

Kumar, A.; Biebuyck, H. A. & Whitesides, G. M. (1994) *Langmuir*, Vol. 10, pp. 1498

Kumar, S.; Chaudhury, K.; Sen, P. & Guha1, S. K. (2005) Atomic force microscopy: a powerful tool for high-resolution imaging of spermatozoa, *Journal of Nanobiotechnology,* Vol. 3, N°9, pp. 1-6

Lavrich, D. J.; Wetterer, S. M.;. Bernasek, S. L. & Scoles, G. (1998) *J. Phys. Chem. B*, Vol. 102, pp. 3456-3465

Levicky, R.; Herne, T. M.; Tarlov, M. J. & Satija S. K. (1998) Using self assembly to control the structure of DNA monolayers on gold : a neutron reflectivity study, *J. Am. Chem. Soc.*, Vol. 120, pp. 9787

Lisdat, F.; Ge, B. & Scheller, F. W. (1999) *Electrochem. Commun*., Vol. 1, pp. 65-68

Lyubchenko, Y. L.; Blankenship, R. E.; Gall, A. A.; Lindsay, S. M.; Thiemann, O.; Simpson, L. & Shlyakhtenko, L. S. (1996) *Scanning Microsc. Suppl.*, Vol. 10, pp. 97

Lyubchenko, Y.L.; Shlyakhtenko, L.S. & Ando, T. (2011) Imaging of nucleic acids with atomic force microscopy, Methods, Vol. 54, N°2, pp. 274-283.

Madou, M. (2002) *Fundamentals of Microfabrication: The Science of Miniaturization*, CRC, pp. 62–63

Magonov, S. N. & Reneker, D. H.. (1997a) Characterization of polymer surfaces with atomic force microscopy, *Annu. Rev. Mater. Sci*., Vol. 27, pp. 175–222

Magonov, S. N.; Elings, V. & Whangbo, M-H. (1997b) Phase imaging and stiffness in tapping mode AFM, *Surf. Sci.,* Vol. 375, pp. 385–391

Mamin, H. J.; Birk, H.; Wimmer, P. & Rugar, D. (1994) High-speed scanning-tunneling-microscopy—principles and applications, *J. Appl. Phys.,* Vol. 75, pp. 161–168

Maslova, M. V.; Gerasimova, L. G. & Forsling, W. (2004) *Colloid J., Vol. 6*, pp. 322–328

Möller, C.; Allen, M.; Elings, V.; Engel, A. & Müller, D.J. (1999) Tapping-Mode Atomic Force Microscopy Produces Faithful High-Resolution Images of Protein Surfaces, *Biophys. J.,* Vol. 77, pp. 1150–1158

Montanari, A. & Mézard, M. (2000) Hairpin Formation and Elongation of Biomolecules, *Phys. Rev. Lett.*, Vol. 86, pp. 2178

Moreno-Herrero, F.; Colchero, J. ; Gomez-Herrero, J.; & Baro, A. M. (2004) Atomic force microscopy contact, tapping, and jumping modes for imaging biological samples in liquids, *Physical Review E*, Vol. 69, pp.031915

Mourougou-Candoni, N.; Naud, C. & Thibaudau, F. (2003) Adsorption of thiolated oligonucleotides on gold surfaces: An atomic force microscopy study, *Langmuir*, Vol. 19, pp. 682-686

Mourougou-Candoni, N. & Thibaudau, F. (2009) Formation of aminosilane film on Mica, *J. Phys. Chem. B,*Vol. 113, pp. 13026–13034

Müller, D. J.; Fotiadis, D.; Scheuring, S.; Muller, S. A. & Engel, A. (1999) Electrostatically balanced subnanometer imaging of biological specimens by atomic force microscope, *Biophys J.*, Vol. 76, pp. 1101–11

Nuzzo, R. G. & Allara, D. L. (1986) *J. Am. Chem. Soc,*. Vol. 105, pp. 4481

Ohnesorge, F. & Binnig, G. (1993) True atomic resolution by atomic force microscopy through repulsive and attractive forces, *Science,* Vol. 260, pp. 1451–1456

Park, J.K. & Moon, W. K. (2011) Development of XY scanner with minimized coupling motions for high-speed atomic force microscope, *Journal of central south inversity of technology*, Vol.18, N°3, pp. 697-703

Peterlinz, A.; Georgiadis, M.; Herne, T. M.; Tarlov, M. J. (1997) *J. Am. Chem. Soc.*, Vol. 119, pp. 3401-3402

San Paulo, A. & Garcia, R. (2000) High-resolution imaging of antibodies by tapping-mode atomic force microscopy: attractive and repulsive tip–sample interaction regimes , *Biophys. J.,* Vol. 78, pp. 1599–605

Schierbaum, K.; Weiss, T.; Van Velzen, E. T.; Engbersen, J.; Reinhoudt, D. & Cöpel, W. (1994) *Science*, Vol. 265, pp. 1413

Schwartz, D. K.; Steinberg, S.; Israelachvili, J. & Zasadzinski, J. A. N. (1992) *Phys. Rev. Lett.*, Vol. 69, pp. 3354

Schwartz, D.K. (2001) Mechanisms and Kinetics of Self-Assembled Monolayer Formation, *Annu. Rev. Phys. Chem.,* Vol. 52, pp. 107–137

Seah, M. P. & Dench, W. A. (1979) *Surf. Interface Anal., Vol. 1*, pp. 2

Shlyakhtenko, L. S.; Gall, A. A.; Weimer, J. J.; Hawn D. D. & Lyubchenko, Y. L. (1999) *Biophys. J.*, Vol. 77, pp. 568-576

Song, X.; Zhai, J.; Wang, Y. & Jiang, L. (2006) *J. Colloid Interface Sci.*, Vol. 298, pp. 267

Sugawara, Y.; Ohta, M.; Ueyama, H. and Morita, S. (1995) *Science,* Vol. 270, pp. 1646

Steel, A. B.; Herne, T. M. & Tarlov, M. J. (1998) *Anal. Chem.*, Vol. 70, pp. 4670-4677

Sugimara, H.; Hozumi, A.; Kayemana, T. & Takai, O. (2002) *Surf. Interface Anal.*, Vol. 24, pp. 550

Sulchek, T.; Yaralioglu, G. G.; Quate, C. F.; & Minne, S. C. (2002) Characterization and optimisation of scan speed for tapping-mode atomic force microscopy, *Rev. Sci. Instrum.,* Vol. 73, pp. 2928–2936

Sulchek, T.; Hsieh, R.; Adams, J. D.; Yaralioglu, G. G.; Minne, S. C.; Quate, C. F.; Cleveland, J. P.; Atalar, A. & Adderton, D. M. (2000) High-speed tapping mode imaging with active Q control for atomic force microscopy, *Appl. Phys. Lett., Vol.* 76, pp. 1473–1475

Tamayo, J. & Garcia, R. (1996) Deformation, contact time, and phase-contrast in tapping mode scanning force microscopy, *Langmuir* , Vol. 2, pp. 4430–4435

Tamayo, J. & Garcia, R. (1997) Effects of elastic and inelastic interactions on phase-contrast images in tapping-mode scanning force microscopy, *Appl. Phys. Lett.,* Vol. 7, pp. 1 2394–12396

Tamayo, J.; Humphris, A. D. L. & Miles, M. J.; (2000) Piconewton regime dynamic force microscopy in liquid, *Appl. Phys. Lett.,* Vol. 77, pp. 582–584

Tamayo, J.; Humphris, A. D. L.; Owen, R. J.; & Miles, M. J. (2001) High-Q dynamic force microscopy in liquid and its application to living cells, *Biophys. J.,* Vol. 81, pp. 526–37

Tätte, T.; Saal, K.; Kink, I.; Kurg, A.; Lohmus, R.; Mäeorg, U.; Rahi, M.; Rinken, A. & Lohmus, A. (2003) *Surf. Sci.,* Vol. 532, pp. 1085–1091

Tinland, B.; Pluen, A.; Sturm, J. & Weill, G. (1997) *Macromolecules* , Vol. 30, pp. 5763-5765

Trens, P.; Denoyel, R. & Rouquerol, J. (1995) *Langmuir* 1995, Vol. 11, pp. 551–554

Ulman, A. (1991) *An Introduction to Ultrathin Organic Films: From Langmuir–Blodgett to self-assembly*; Academic Press: Boston, MA

Vandenberg, E. T.; Bertilson, L.; Liedberg, B.; Uvdal, K.; Erlandsson, R.; Elwing, H. & Lundstrom, I. (1991) *J. Colloid Interface Sci.*, Vol. 17, pp. 103

Venkataramanan, M.; Skanh, G.; Bandyopadhyay, K.; Vijayamohanan, K. & Pradeep, T. (1999) *J. Colloid. Interface Sci.,* Vol. 212, pp. 553

Vos, J. G.; Forster, R. J. & Keyes T. A. (2003) *Interfacial Supramolecular Assemblies*. Wiley, pp. 88–94.

Vrancken, K. C.; Possemiers, K.; Van der Voort, P. & Vansant, E. F. (1995) *Colloid Surf., A* , Vol. *98*, pp. 235

Walters, D. A.; Cleveland, J. P.; Thomson, N. H.; Hansma, P. K.; Wendman, M. A.; Gurley, G. & Elings, V (1996) Short cantilevers for atomic force microscopy, *Rev. Sci. Instrum.,* Vol. 67, pp. 3583–3590

White, L. D. and Tripp, C. P. (2000) *J. Colloid Interface Sci.*, Vol. 232, pp. 400–407

Wnek, G. & Bowlin, G. L. (2004) *Encyclopedia of Biomaterials and Biomedical Engineering*. Informa Healthcare. pp. 1331-1333.

Wong, S. S.; Harper, J. D.; Lansbury, P. T. & Lieber, C. M. (1998a) Carbon nanotube tips: high-resolution probes for imaging biological systems, *J. Am. Chem. Soc.,* Vol. 120, pp. 603–604

Wong, S. S.; Joselevich, E.; Woolley, A. T.; Cheung, C-L. & Lieber C. M. (1998b) Covalently functionalized nanotubes asnanometer-sized probes in chemistry and biology, *Nature,* Vol. 394, pp. 52–5

Woolley, A.T. (2004) Biofunctionalization of carbon nanotubes for atomic force microscopy imaging, *Methods in molecular biology*, Vol. 283, pp. 305-319

Yang, Y.; Zhou, R.; Zhao, S.; Li, Q. & Zheng, X. (2003) *J. Mol. Catal. A: Chem.,*Vol. 192, pp. 303

Zhang, Y.; Zhou, H. & Ou-Yang, Z. C. (2001) Stretching Single-Stranded DNA: Interplay of Electrostatic, Base-Pairing, and Base-Pair Stacking Interactions, *Biophys. J.*, Vol. 81, pp. 1133

Zhang, F. & Srinivasan, M. P. (2004) *Langmuir,* Vol. 20, pp. 2309

Zhao, J.; Guo, T.; Ma, L.; Fu, X. & Hu, X.T. (2011) Metrological atomic force microscope with self-sensing measuring head, *Sensors and actuators A-physical*, Vol.167, N°2, pp. 267-272

IntechOpen

IntechOpen

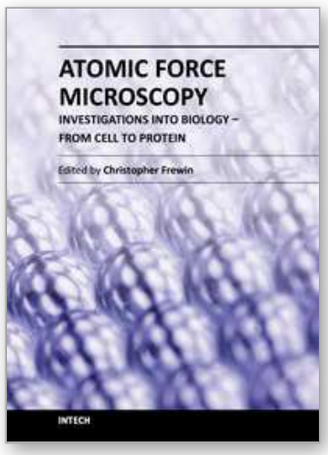

Atomic Force Microscopy Investigations into Biology - From Cell to Protein

Edited by Dr. Christopher Frewin

ISBN 978-953-51-0114-7
Hard cover, 354 pages
Publisher InTech
Published online 07, March, 2012
Published in print edition March, 2012

The atomic force microscope (AFM) has become one of the leading nanoscale measurement techniques for materials science since its creation in the 1980's, but has been gaining popularity in a seemingly unrelated field of science: biology. The AFM naturally lends itself to investigating the topological surfaces of biological objects, from whole cells to protein particulates, and can also be used to determine physical properties such as Young's modulus, stiffness, molecular bond strength, surface friction, and many more. One of the most important reasons for the rise of biological AFM is that you can measure materials within a physiologically relevant environment (i.e. liquids). This book is a collection of works beginning with an introduction to the AFM along with techniques and methods of sample preparation. Then the book displays current research covering subjects ranging from nano-particulates, proteins, DNA, viruses, cellular structures, and the characterization of living cells.

How to reference

In order to correctly reference this scholarly work, feel free to copy and paste the following:

Nadine Mourougou-Candoni (2012). Tapping Mode AFM Imaging for Functionalized Surfaces, Atomic Force Microscopy Investigations into Biology - From Cell to Protein, Dr. Christopher Frewin (Ed.), ISBN: 978-953-51-0114-7, InTech, Available from: http://www.intechopen.com/books/atomic-force-microscopy-investigations-into-biology-from-cell-to-protein/tapping-afm-imaging-system-for-molecule-adsorption-on-surface

InTech Europe
University Campus STeP Ri
Slavka Krautzeka 83/A
51000 Rijeka, Croatia
Phone: +385 (51) 770 447
Fax: +385 (51) 686 166
www.intechopen.com

InTech China
Unit 405, Office Block, Hotel Equatorial Shanghai
No.65, Yan An Road (West), Shanghai, 200040, China
中国上海市延安西路65号上海国际贵都大饭店办公楼405单元
Phone: +86-21-62489820
Fax: +86-21-62489821

© 2012 The Author(s). Licensee IntechOpen. This is an open access article distributed under the terms of the Creative Commons Attribution 3.0 License, which permits unrestricted use, distribution, and reproduction in any medium, provided the original work is properly cited.

IntechOpen

IntechOpen